

*COVRA Rocksalt Sealing Project*

**Long-term porosity-permeability evolution in and around backfilled  
openings in a radioactive waste repository in rock salt**

**Experimental investigation on the effect of stress,  
grain size (distribution) and porosity on compaction  
rates in granular rock salt backfill and implications  
for sealing timescales of a radioactive waste  
repository**

## **Phase 2 Deliverable**

B.G.A. van Oosterhout (b.g.a.vanoosterhout@uu.nl),  
S.J.T. Hangx, C.J. Spiers, J.H.P. de Bresser  
HPT Laboratory, Faculty of Geosciences,  
Utrecht University, The Netherlands

*Work carried out in the period May 2022-May 2023*



# Contents

<b>Abstract</b>	<b>3</b>
<b>1 Introduction</b>	<b>4</b>
1.1 Background . . . . .	4
1.2 Problem . . . . .	4
1.3 The aims of the present research . . . . .	5
<b>2 Method</b>	<b>6</b>
2.1 General approach . . . . .	6
2.2 Sample preparation . . . . .	6
2.3 Apparatus and experimental method . . . . .	7
2.3.1 Deformation Apparatus . . . . .	7
2.3.2 Experimental procedure . . . . .	7
2.3.3 Stress relaxation experiments . . . . .	8
2.4 Permeability measurements . . . . .	9
2.5 Data acquisition and processing . . . . .	9
2.5.1 General aspects . . . . .	9
2.5.2 Time series analysis technique . . . . .	9
2.6 Accounting for uncertainties . . . . .	9
2.6.1 Uncertainties in porosity . . . . .	9
2.6.2 Uncertainties in permeability . . . . .	10
<b>3 Results</b>	<b>10</b>
3.1 Mechanical data . . . . .	10
3.1.1 Effect of porosity . . . . .	12
3.1.2 Effect of grain size . . . . .	13
3.1.3 Results of experiments on mixtures . . . . .	16
3.2 Permeability data . . . . .	18
<b>4 Discussion</b>	<b>18</b>
4.1 Deformation mechanisms . . . . .	18
4.1.1 Deformation mechanism at low stress . . . . .	19
4.1.2 Required adjustments to pressure solution creep model . . . . .	21
4.1.3 Deformation mechanism at high stress . . . . .	22
4.2 A composite flow law for backfill compaction . . . . .	23
4.3 Compaction creep in mixtures with a distributed grain size . . . . .	27
4.3.1 A model for compaction creep in mixtures: theory . . . . .	28
4.3.2 A model for compaction creep in mixtures: results . . . . .	29
4.4 The permeability of compacted rock salt . . . . .	32
4.5 A model for coupled convergence of a backfilled repository . . . . .	33
4.5.1 The effect of backfill grain size on repository convergence . . . . .	33
4.5.2 Other effects on repository convergence . . . . .	38
<b>5 Recommendations</b>	<b>38</b>
<b>6 Future plans</b>	<b>39</b>
<b>7 Conclusions</b>	<b>39</b>
<b>8 Acknowledgements</b>	<b>40</b>
<b>9 References</b>	<b>40</b>

## Abstract

Rock salt formations are widely considered as a host rock for radioactive waste disposal facilities. Galleries, boreholes and other openings in such a repository are expected to be backfilled with granular crushed rock salt that is expected to compact during convergence of the repository walls and ultimately attain a permeability comparable to that of natural, undisturbed rock salt. The timescales required to achieve a low porosity/permeability are of importance in assessing the sealing capacity and necessary lifetime of the disposal packaging (i.e. the first barrier ensuring containment). There is a lot of data available on the compaction creep rate of backfill at high and intermediate porosity, but at low backfill porosity most of the available data is obtained at stresses higher than expected during in-situ convergence. In addition, most of the data is obtained for aggregates consisting of single grain size fractions or in aggregate mixtures with a distributed grain size, containing multiple grain size fractions, but the contribution of individual grain size classes to the overall compaction rate in these mixtures is not well understood. Hence, there is uncertainty whether the in-situ compaction and healing/sealing mechanisms are actually identified and quantified in previous experiments. This results in uncertainty in extrapolating the results of these mixtures beyond laboratory conditions towards lower stresses.

In this study, we have carried out stress relaxation experiments in 1D compaction mode on granular salt on single grain size fractions and mixtures with a distributed grain size. Stress relaxation experiments allow for investigation of the compaction rate under a wide range of stresses, for a near-constant aggregate porosity. Samples were pre-compacted rapidly to a fixed porosity in the range of 30-1%. The stress on the sample was then allowed to relax and strain rates were obtained at a continuously decaying stress. The effects of pore fluid, applied stress, grain size and porosity were systematically investigated. In the brine-saturated samples, at low stress ( $< 5\text{-}30$  MPa, depending on grain size and porosity) the compaction creep rate was linearly proportional to stress and showed a (near) cubic inverse dependence on grain size ( $d^{-2.5 \text{ to } -3}$ ), which is attributed to pressure solution. At higher stresses, a transition to non-linear creep was observed, with apparent power law stress exponents ( $n$ ) of 3-7. This is generally attributed to dislocation dominated mechanisms, but this does not explain the grain size dependence ( $d^{0 \text{ to } 2}$ ) observed in our study. Hence, we have derived an empirical law that describes the grain size sensitivity observed in this domain.

We have developed two models to predict the upper and lower bound for the compaction rate resulting from pressure solution creep in a salt aggregate mixture, based on its grain size distribution and the rates obtained from single grain size fraction experiments. In this study, we show that the geometric mean of these two models can be used to predict the creep rate of a mixture. However, uncertainties remain whether this can be applied to mixtures with a much broader grain size distribution.

Overall, our results show a larger decrease in strain rates at lower aggregate porosity values than predicted by the porosity dependence observed at higher porosity values. Based on the experimental results we have modified existing constitutive equations to include this decrease in strain rates at low porosity ( $< 10\%$ ). We have used these equations to assess the coupled-convergence of a repository, containing a few percent of brine, to predict the evolution of stress, porosity and compaction rate of backfill as a function of time. This allows us to predict the timescale for sealing. Results show that for fine-grained backfill ( $< 1$  mm), pressure solution creep is the sole mechanism during in-situ convergence/backfill compaction. Based on the experimental results in this study, a backfill porosity of 1% is reached after 300 years for a grain size of 0.3 mm up to 8000 years for a grain size of 3.0 mm.

# 1 Introduction

## 1.1 Background

Rock salt formations are widely considered as a suitable host rock for a geological repository for nuclear waste, because of its natural low permeability ( $< 10^{-21} \text{ m}^2$ ). Another advantage of selecting rock salt as a host rock for disposal of nuclear waste is that creep processes in rock salt operate relatively fast, which ensures that porosity and permeability evolve to low values following mechanical damage (e.g. Langer 1999), such that its sealing capacity is restored. The concept for safe disposal in rock salt is based on a system consisting of multiple engineered barriers, which include: (1) an engineered barrier (e.g. the disposal package consisting of steel/concrete canisters containing the radioactive waste), (2) a geo-engineered barrier (i.e. the galleries, boreholes, shafts and other openings filled with backfill) and (3) a geological barrier (i.e. the surrounding host rock seal) (Pusch 2009). Note that these combined barriers provide the required long-term containment, but that each barrier covers a different timescale in the disposal evolution.

In the case of a repository in rock salt, it is planned to use crushed rock salt as backfill. Crushed salt is suitable for backfilling, because the same creep mechanisms that allow for fast creep in dense rock salt allow for fast compaction creep of the backfill. In addition, crushed salt is readily available as it can be obtained from excavated material derived from the creation of the repository itself. Furthermore, the backfill provides stabilisation to the surrounding host rock and allows for the conduction of heat generated from the decay of the nuclear waste (Holcomb and Hannum 1982).

It is expected that backfilled openings will ultimately converge and that the crushed backfill will compact to reach a state in which its properties, specifically the porosity and the permeability, are comparable to that of undisturbed rock salt (i.e. the surrounding host rock). This in turn will delay potential transport of radionuclides out of the repository. The barrier function of the disposal containers and seals can no longer be guaranteed after 1000-10.000 years, due to corrosion. Provided sufficient cavity closure and porosity-permeability reduction in the backfill can be achieved, at this stage the backfilled zones take over the function as a barrier for the longer term (1000 - 1 million years). Hence a key aim of research on salt repository integrity is to obtain models that can reliably predict the long-term porosity-permeability evolution of the backfill in converging repository openings. The timescale on which a given porosity-permeability reduction in the backfill is achieved, depends on how the convergence rate of an opening decreases as the resistance to compaction offered by the densifying backfill increases. Hence a full understanding of the creep processes operating in the surrounding host rock and the backfill is required to accurately predict the porosity-permeability evolution of the backfill.

## 1.2 Problem

The compaction behavior of crushed rock salt is controlled by a combination of mechanisms and depends on the properties of the backfill (mineralogy and grain size) and the in-situ conditions (stress state, temperature, brine availability/relative humidity, presence of gas). Under the in-situ conditions relevant for a converging backfilled opening in rock salt, the state of stress within the backfill will be determined by the mechanical coupling between the convergence creep of the surrounding salt rock and the compaction creep behavior of the backfill. In experiments addressing backfill compaction behavior, controlled stress or controlled compaction rate boundary conditions are usually imposed to obtain a compaction law that can be applied in numerical simulations.

The compaction rate significantly decreases with decreasing porosity and hence many experiments increase the mean stress in steps (e.g. Kröhn et al. 2012; Czaikowski et al. 2012): (1) because during convergence it is expected that the mean stress will increase as the backfill compacts and its resistance increases; (2) to get strain rates that can be readily measured in the laboratory and (3) to reach a low porosity ( $\ll 10\%$ ) in a single experiment. In many experiments on crushed salt, the stress is generally increased to around 20 MPa at intermediate porosity values (10-15%). However, it is expected that stresses above 10-15 MPa are not reached at the depth of a general repository (700-800 m) and a stress of 10-15 MPa is only reached at the very final stages of compaction at 3-10% porosity (Kröhn et al. 2012) (depending on grain size of the backfill, brine availability and temperature). By doing experiments at unrealistically high stresses, there is a chance that the mechanism of deformation, and hence stress-strain

rate relationships, observed in the lab are relevant for those operating under realistic in-situ conditions.

In the presence of water, especially at low stresses ( $< 10$  MPa), there is significant evidence that compaction creep is accelerated (Spiers et al. 1990). This is attributed to pressure solution creep, which results in dissolution at highly stressed contacts, diffusion through the pore fluid and precipitation at pore walls. Hence adding brine will accelerate compaction, and thus likely also sealing, of the backfill. However, the addition of brine will also accelerate corrosion of the canisters, limiting their lifetime, and hence requires the backfill permeability to be (near) impermeable at an earlier stage. Therefore, many disposal concepts in rock salt consider adding only a few percent of brine to speed up the compaction process, while simultaneously limiting the effect of corrosion. Alternatively, dry salt could be used close to the canisters, while wetted salt may be used further away from the canisters. There is significant evidence that a few percent of brine present is sufficient to accelerate creep to rates approaching brine-saturated conditions (Kröhn et al. 2012), but there are uncertainties in the amount of brine that will be available in the repository in-situ due to inflow or expulsion from the surrounding host rock (Guiltinan et al. 2020).

Rock salt is hygroscopic and will adsorb water from the air until an equilibrium humidity of 75% is reached. There is evidence that the surface diffusivity, which is the rate-controlling parameter for pressure solution, can be relatively high and of similar magnitude as for saturated conditions or up to 1-2 orders of magnitude lower than for saturated conditions (e.g. Koelemeijer et al. 2012). Therefore, even without adding liquid brine, the rate of pressure solution is lower than under brine-saturated conditions, but can be expected to play an important role in the compaction under humid conditions.

Many experiments on compaction creep in rock salt are either performed on samples with a very narrow grain size distribution ( $< 0.1$  mm variation, from now on referred to as a 'single grain size' fraction) (e.g. Zhang et al. 2007; Spiers et al. 1990) or on a mixture with a known (broader) grain size distribution (e.g. Kompass mixture Kröhn et al. 2012; Czaikowski et al. 2012). For such mixtures, grain sizes typically range from 0.1 mm-10 mm. Compaction experiments on single grain size fractions show that the strain rate ( $\dot{\epsilon}$ ) very strongly depends on grain size ( $d$ ), with rates increasing in smaller grain sizes ( $\dot{\epsilon} \propto d^3$ ), especially at low stresses where pressure solution dominates over processes controlled by the movement of dislocations.

Assuming that the stress is distributed homogeneously, it can be expected that the overall (sample-scale) compaction rate is controlled by the smaller grain size fractions. Conversely, if the strain rate is distributed homogeneously, the overall compaction rate is controlled by the larger grain size fractions. Nevertheless, nearly all models (Callahan et al. 1998; Spiers et al. 1990; Czaikowski et al. 2012; Kröhn et al. 2012) use a single grain size as input parameter, by simply taking the average grain size of a mixture, or select a grain size value such that the model fits the experimentally observed rates. However, this makes extrapolation beyond laboratory conditions questionable. Furthermore, it relies on using the exact same grain size distribution in a real repository as the one used in the experiments, to allow for extrapolation of the lab data as the contribution of each individual grain size fraction on the overall rate is unknown.

### 1.3 The aims of the present research

In this study, we aim to investigate the effect of stress, porosity and grain size on the compaction rate of granular rock salt. In addition we aim to investigate the effect of grain size distribution (single grain size fraction versus distributed grain size/mixture) on creep rates. Therefore, we have performed stress relaxation 1D-compaction experiments on pre-compacted porous granular salt to obtain rheological data at porosity values in the range of 30-1%. Stress relaxation experiments allow for investigation of compaction rates under a wide range of stresses, while aggregate porosity stays nearly constant. Mechanism-based microphysical models, describing the compaction processes, are developed for both aggregates consisting of single grain size fractions and mixtures. In particular, these models describe the behavior at low stresses, relevant for in-situ convergence, which is the domain where pressure solution creep is expected to dominate.

In addition, we have developed an analytical solution for the mechanical coupling between the host rock and the backfill to evaluate timescales for sealing. In addition, we evaluated whether the conditions at which the experiments were obtained are relevant for the in-situ conditions expected during conver-

gence and to assess whether the assumption that pressure solution creep will dominate can be justified.

## 2 Method

### 2.1 General approach

The experiments reported here consist of 1D (oedometric) compaction experiments performed on crushed/sieved salt with a grain size of up to 0.45 mm. Experiments are performed primarily under brine-saturated (wet) conditions. The samples were pre-compacted at a relatively rapid constant strain rate, until a desired porosity was reached in the range of 30-1%. This pre-compaction phase was followed by a stress relaxation phase to determine the strain rate as a function of decaying stress at near constant porosity. After each stress relaxation phase, the aggregate permeability at that porosity was investigated. The sample was subsequently pre-compacted to the next desired porosity and the procedure was repeated.

### 2.2 Sample preparation

Samples were prepared by manually sieving reagent grade sodium chloride (Merck, 99.9% pure) into fractions of  $115 \pm 9 \mu\text{m}$ ,  $137.5 \pm 12.5 \mu\text{m}$ ,  $165 \pm 15 \mu\text{m}$ ,  $225 \pm 25 \mu\text{m}$ ,  $325 \pm 25 \mu\text{m}$ ,  $375 \pm 25 \mu\text{m}$  and  $450 \pm 50 \mu\text{m}$ . To determine the effect of grain size distribution, three mixtures were prepared (see Figure 1). Mixtures 1 and 2 consisted of a combination of the  $137.5 \mu\text{m}$  and  $450 \mu\text{m}$  grain size fraction in respectively a 50-50 volume ratio and 75-25 volume ratio. Mixture 3 was based on a log-normal volume distribution with a mean grain size of  $225 \mu\text{m}$  and a standard deviation of 0.45. Using a wide range of sieves from  $71 \mu\text{m}$  to  $500 \mu\text{m}$ , a mixture was constructed that approached a continuous distribution characterized by this mean grain size and standard deviation (see Figure 1).

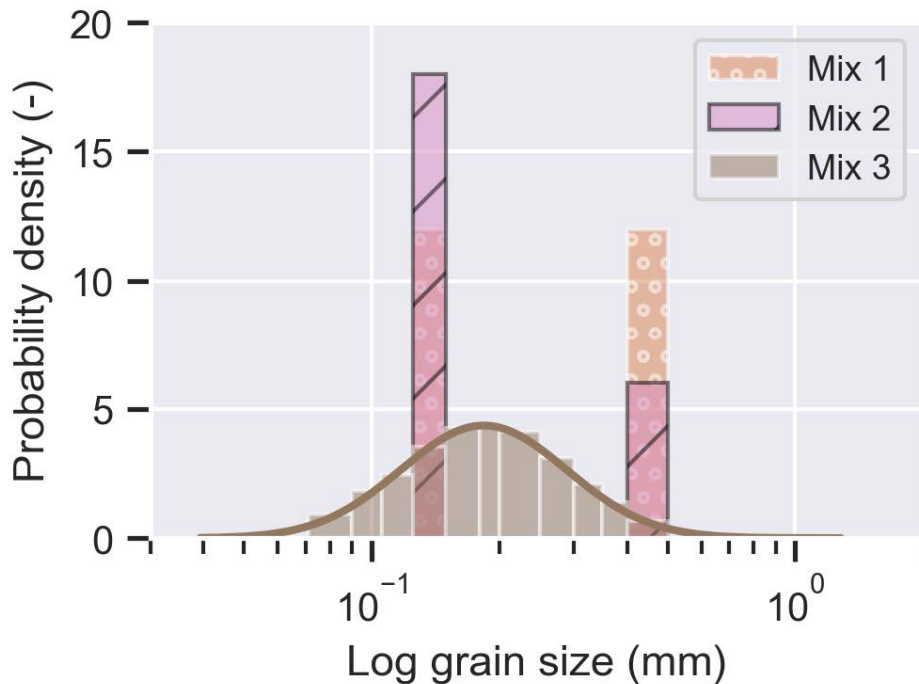


**Figure 1:** Overview of grain size distributions used in this study, as volume probability versus log grain size, for a 50-50% mixture of 137 and 450  $\mu\text{m}$  (Mixture 1), a 75-25 vol% mixture of 137 and 450  $\mu\text{m}$  (Mixture 2), and a log-normal volume distribution with a median of 225  $\mu\text{m}$ , a mode of 183  $\mu\text{m}$  and a standard deviation of 0.45 (Mixture 3). For Mixture 3, a mixture was constructed using the available sieve sizes that approached the same distribution as the continuous distribution (see individual bars).

## 2.3 Apparatus and experimental method

### 2.3.1 Deformation Apparatus

The apparatus used for the compaction experiments (pre-compaction and stress relaxation) consists of a 1D-oedometric compaction vessel, placed in an INSTRON 8862 testing machine. Figure 2 shows a schematic diagram of the compaction vessel and sample assembly. The vessel has an inner diameter of 19.30 mm. The testing machine is equipped with controlled data logging capacities.

A local linear velocity displacement transducer (LVDT) was installed between the top piston and the top of the vessel, to measure the shortening of the sample during compaction. A second LVDT was located in the INSTRON drive unit to measure piston position and was used to determine the absolute length of the sample. The INSTRON testing machine was equipped with a 100 kN load cell, used to determine the load and change of load during the relaxation experiments. For some of the later experiments, a different bottom piston was used that contained strain gauges to measure the load exerted by the sample on the bottom piston. This was done to obtain insight into the friction between the sample and vessel wall, which could impact compaction. Two thermocouples were used to measure the temperature, of which one measured the temperature of the outer side of the vessel, close to the furnace, while the other was embedded in the vessel wall to measure sample temperature. The top and bottom piston contain a central bore to allow fluid access to and flow through the sample. The whole assembly (INSTRON load frame, compaction vessel and tubing) was placed inside temperature-controlled box at a constant temperature of 28°C. This was done to reduce thermal expansion and contraction of the whole set-up due to temperature fluctuations.

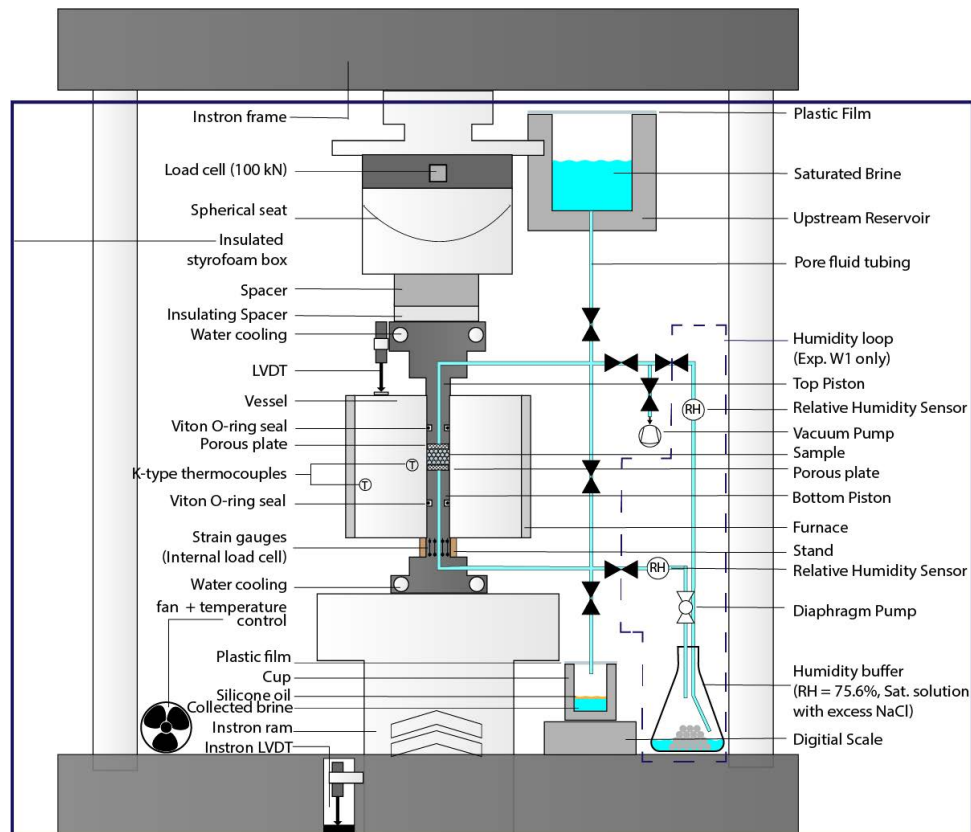


**Figure 2:** Schematic diagram of the 1D compaction vessel used in the present experiments (after Zhang et al. (2007)). Note that the part highlighted with the dashed line was only used and connected for experiment W1 (see Table 1).

### 2.3.2 Experimental procedure

For each experiment a fixed weight of sodium chloride (6.24 g) was used. Together with the absolute length of the sample it was possible to calculate sample porosity, at any time step. Prior to emplacing

**Table 1:** List of compaction experiments on pre-compacted granular salt samples. All experiments were performed at room temperature on brine-saturated samples ( $P_f$ ), unless indicated otherwise.

Exp	Grain size ( $\mu\text{m}$ )	Porosity at start of relaxation phases (%)
RC1	$325 \pm 25$	26.3, 15.3, 10.2, 5.2 and 1.5
RC2	$137 \pm 13$	26.3, 15.3, 10.2, 5.2 and 1.5
RC3	$225 \pm 25$	20.3, 16.3, 10.3, 5.0 and 2.1
RC4	$115 \pm 10$	20.3, 15.3, 10.2, 5.0 and 1.5
RC5	$165 \pm 15$	19.8, 14.8, 10.3, 4.8 and 1.1
RC6	$450 \pm 50$	19.9, 14.8, 9.8, 4.8 and 1.0
M1	Mix1	19.7, 14.7, 9.8 and 4.9
M2	Mix2	19.8, 14.7, 9.8 and 4.7
M3	Mix3	19.8, 14.8 and 4.8
W1 <sup>1</sup>	$165 \pm 15$	20.2, 15.4, 10.5 and 5.0

the sample into the vessel, a layer of Boron Nitride was sprayed on the inner side of the vessel to reduce the friction between sample and vessel. The bottom piston was inserted into the vessel and a porous plate of Monel steel was placed on top. The sodium chloride sample was funneled into the vessel and a second porous plate was placed on top of the sample, before inserting the top piston.

All pre-compaction was performed on lab-dry material, except W1, at a constant strain rate of  $5 \cdot 10^{-5} \text{ s}^{-1}$  until a porosity of 25%. The assembly was subsequently unloaded, evacuated and flooded with saturated brine, before pre-compaction to 20%, followed by a direct stress relaxation test under drained conditions (i.e. the brine was connected to an upstream reservoir with a free surface to maintain a constant pressure during the experiment, while preventing evaporation). Further stress relaxation tests on the same sample were performed at (roughly) 15, 10, 5 and 1% porosity (see Table 1).

### 2.3.3 Stress relaxation experiments

The stress relaxation test method used in this study is commonly used in rock deformation experiments to obtain steady state creep data at low strain rates within relatively shorter measuring times (Rutter and Mainprice 1978; Lee and Hart 1971). The technique involves the interruption of a conventional compaction test by switching off the motor of the testing machine (i.e. active displacement by the loading frame is stopped). From that moment on, the sample will continue to compact under the applied load, but as the sample compacts, the load will decay and as a result the testing machine elastically expands. The small displacements occurring at the level of the sample due to this relaxation can be directly measured using the external LVDT, but part of the sample strain is inferred from the elastic strain of the apparatus, which is determined during a calibration. In addition, to obtain the plastic strain of the sample, the sample strain has to be corrected for the elastic strain of the sample due to the decrease in stress during relaxation. To determine the plastic strain rate in the sample ( $\dot{\epsilon}_p$ ) and its relation to the rate of axial stress change has to be taken into account using equation:

$$\dot{\epsilon}_p = \dot{\epsilon}_m - \left[ \frac{A}{L(t)} C_a(F) + C_s \right] \frac{d\sigma}{dt} \quad (1)$$

where  $\dot{\epsilon}_m$  is the strain rate directly measured by the local LVDT,  $A$  is the cross sectional area of the sample ( $\text{m}^2$ ) and  $L$  is the sample length (m).  $C_a$  is the elastic compliance of the testing machine ( $\text{mm/N}$ ), obtained from a calibration run without a sample as a function of applied force, and  $C_s$  is the elastic compliance of the sample ( $\text{MPa}^{-1}$ ) measured before and after each relaxation run.  $\frac{d\sigma}{dt}$  is the rate of change of effective stress with time ( $\text{MPa s}^{-1}$ ). The effective stress is the applied axial stress measured with respect to 1 atm pressure of the pore fluid phase ( $\sigma_e = \sigma - P_f$ ).

Another advantage of using stress relaxation experiments is that one can obtain the relation between stress and plastic flow rate of the sample, within a single test. In addition during stress relaxation the changes in porosity are relatively small, such that one can obtain the strain rate at a near constant porosity. A key issue with interpreting mechanical data of stress stepping tests is that differences in strain rate will always result in reaching a certain porosity at a different moment in time (and hence stress) during the experiment. This makes a direct comparison between experiments challenging and makes it

virtually impossible to isolate the effect of porosity or stress on compaction rate, without assuming that one knows the exact effect of the other in advance.

## 2.4 Permeability measurements

Permeability measurements were carried out at the end of each relaxation test using saturated brine as pore fluid. The permeability was measured using a "constant head" setup with an elevation head of 0.38 m (4480 Pa). The volume of brine permeating through the sample was collected at the downstream end. The mass of outflowing brine was measured and converted into volume to obtain a flow rate.

$$\kappa = \mu \frac{Q L_s}{A \rho g h} \quad (2)$$

in which  $\kappa$  is the permeability in  $\text{m}^2$ ,  $\mu$  is the dynamic viscosity of the brine ( $\text{Pa s}^{-1}$ ) and  $Q$  is the fluid flux traversing the sample ( $\text{m}^3\text{s}^{-1}$ ).  $A$  and  $L_s$  are respectively the cross sectional area of the sample ( $\text{m}^2$ ) and the sample length (m).  $\rho$  is the density of brine,  $g$  is the gravitational acceleration ( $\text{ms}^{-2}$ ) and  $h$  is the elevation head.  $Q$  was obtained at specific times by smoothing volume collected at the downstream end versus time using linear regression over the entire measurement.

## 2.5 Data acquisition and processing

### 2.5.1 General aspects

A PC equipped with Signal Express logging software was used to log displacement, force and the sample temperature with a logging interval of 1 second. HBM perception software was used to log the voltage of the strain gauges and convert it to internal force exerted on the bottom piston, using a calibration test with a known load. A Python script was used for determining the weight of brine at the downstream end.

### 2.5.2 Time series analysis technique

For the stress relaxation experiments, the change of force with time data was obtained at specific times by smoothing force versus time using a moving average method. This was followed by linear regression using a minimal window of a force drop of 0.1 kN, which was subsequently converted into stress, to obtain  $\frac{d\sigma}{dt}$ . The same approach was used to obtain the strain rate measured by the local LVDT, but using a minimal window of displacement (shortening) of 4  $\mu\text{m}$ . The displacement rate was divided by the length of the sample to obtain the strain rate ( $\dot{\epsilon}_m$ ).

## 2.6 Accounting for uncertainties

### 2.6.1 Uncertainties in porosity

The absolute length of the sample is determined by the position of the LVDT in the INSTRON drive unit. Displacement measurements were corrected for machine distortion using a predetermined 6<sup>th</sup> order polynomial function. Based on these calibrations, the standard error of regression has been determined as 0.015 mm. Using the general approach of taking 1.96 times the standard error (cf. Taylor 1997), the error is 0.0294 mm. This implies an absolute error of  $\pm 0.27\%$  at 20% porosity means a relative error of 1.4% in the calculated porosity, but a relative error of 27% at an aggregate porosity of 1%.

In addition, the above determination of porosity assumes that the density of the solid phase (i.e. of the grains) does not change, which is not entirely true. Assuming that at low porosity (e.g. <5% porosity), the bulk modulus is comparable to that of dense rocksalt ( $K = 20$  GPa), the volumetric strain associated with bulk compaction is given by:  $\epsilon_{ve} = \frac{\sigma}{K}$ . Hence, assuming that all volume reduction is solely the result of pore volume reduction underestimates the porosity. This can be accounted for using:

$$\phi_{\text{corrected}} = \left( \epsilon_{ve} \left( 1 + \frac{\phi}{100} \right) * 100 \right) + \phi \quad (3)$$

in which  $\phi$  is the porosity in %, neglecting any density changes in the solid, and  $\phi_{\text{corrected}}$  is the porosity in % corrected for the change in solid density. At a stress of 100 MPa and a porosity of 1%, this results in an underestimation of porosity by 0.51%. At 10 MPa, this underestimation is reduced to 0.05%.

## 2.6.2 Uncertainties in permeability

The permeability was determined by linear regression of the flow rate versus time (see Section 2.4). For each permeability measurement the standard error of regression was determined ( $\delta Q$ ). Errors due to other sources were estimated assuming that these could be regarded as independent and random. The error in length has already been determined in the previous section. In addition there is some uncertainty in the dynamic viscosity of brine. Here, a dynamic viscosity of  $9.54 \cdot 10^{-3} Pa s^{-1}$  for saturated brine at 28°C has been used (based on Phillips 1981). According to Oldenburg and Pruess (1995) the dynamic viscosity of saturated brine at those temperatures is  $8.90 \cdot 10^{-3} Pa s^{-1}$ , hence the absolute error of viscosity is estimated to be  $6.42 \cdot 10^{-5} Pa s^{-1}$ . The total error in permeability is given by (cf. Taylor 1997):

$$\frac{\delta \kappa}{\kappa} = \sqrt{\left(\frac{\delta Q}{Q}\right)^2 + \left(\frac{\delta \mu}{\mu}\right)^2 + \left(\frac{\delta L}{L}\right)^2} \quad (4)$$

The error of flow rate varies from measurement to measurement, the calculated errors in permeability obtained in this study vary between 11 and 29%.

# 3 Results

## 3.1 Mechanical data

The experiments conducted in this study are listed in Table 1. All the experiments show an increase in relaxation time with decreasing porosity, as demonstrated by their effective (axial) stress versus time behavior (e.g. for a grain size fraction of 137  $\mu m$ , see Figure 3). This figure clearly demonstrates the effect of decreasing porosity on increasing relaxation time. Figure 4 shows the effect of pore fluid and grain size on relaxation time, at an aggregate porosity of 10%. The stress relaxation data can be converted into strain rate using Equation 1. Overall, all experiments show a rapid decrease in plastic strain rate as the stress acting on the sample decays away (Figures 5-6). As aggregate porosity decreases the absolute strain rate decreases with each subsequent relaxation stage, leading to a total reduction in strain rate by three orders of magnitude throughout the whole experiment. When plotted in log stress versus log strain rate space, the slope of these curves show the direct creep rate dependence on the applied stress for the samples tested under various conditions (compare curves and n-value slopes in Figures 5-7-11).

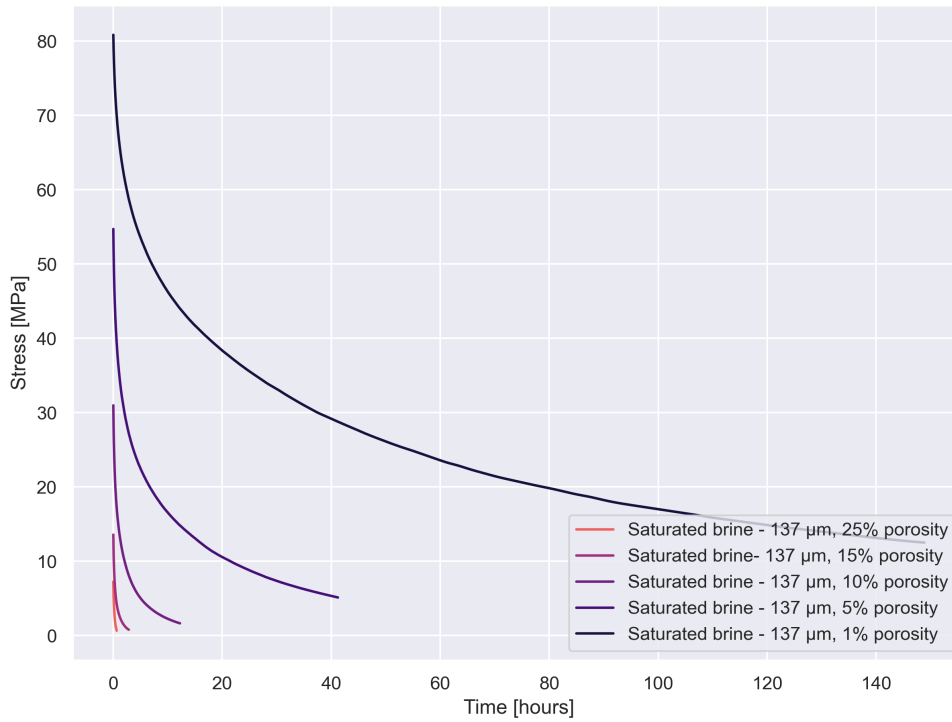


**Figure 3:** Stress relaxation curves (stress versus time) for a single sample with a grain size of  $137 \pm 25 \mu\text{m}$ , for porosity in the range of 25 to 1% ( $\pm 1\%$ ) showing the increase in relaxation time with decreasing porosity.

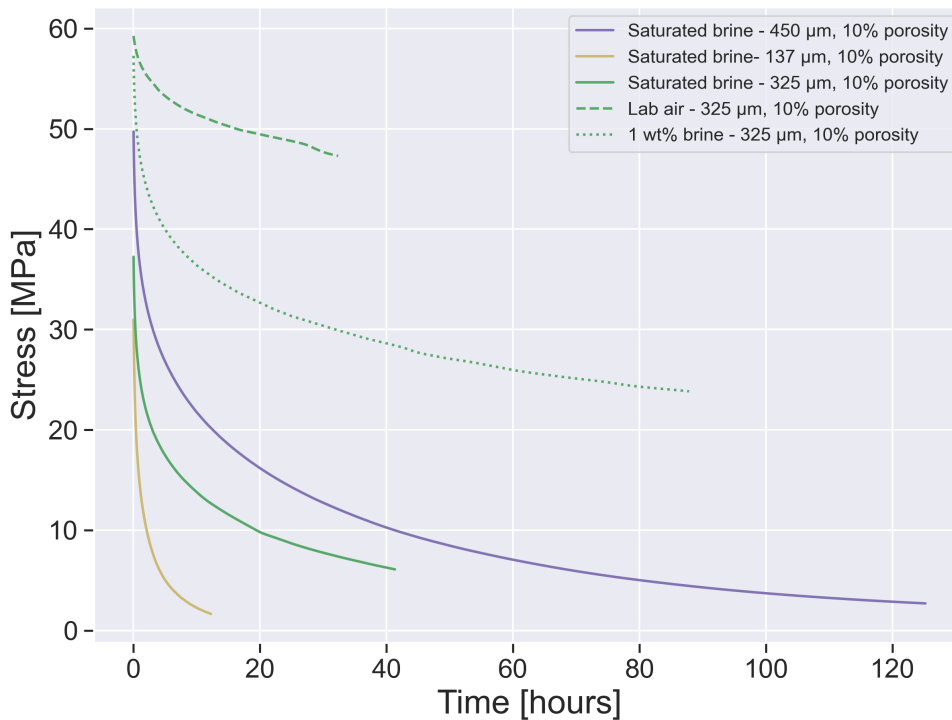


**Figure 4:** Stress relaxation curves (stress versus time) for a range of grain sizes at different conditions, for an aggregate porosity of 10%. Note the acceleration of stress relaxation by changing the chemical environment from lab-air to 1wt% brine and saturated with brine, for an aggregate with a single grain size fraction of  $325 \mu\text{m}$  (green curves). Also note the decrease in relaxation time when reducing the grain size from  $450 \mu\text{m}$  to  $325 \mu\text{m}$  to  $137 \mu\text{m}$  respectively.

### 3.1.1 Effect of porosity

Typically, creep data are described using flow laws that relate stress to strain rate via a power-law function of the form  $\dot{\epsilon} = A\sigma^n$ , in which the  $n$ -value describes the slope and varies depending on the underlying mechanism. In the case of dense materials,  $A$  depends in general on temperature and grain size, while for compaction creep of porous materials  $A$  also depends on porosity, which will decrease with decreasing porosity. In the present samples with the pores flooded with saturated brine (Figures 5-6) a clear transition from steep slopes (high  $n$ -value) to shallow slopes (low  $n$ -value) can be observed when going from high to low stress. Note, that the initial stress for each relaxation phase is purely determined by the stress required during pre-compaction to obtain the desired porosity for the relaxation phase. In general, for the sample with a grain size of  $137 \mu\text{m}$  (Figure 5), the  $n$ -value gradually changes from 2-6 at high stress (power-law or non-linear stress-dependence) to around 1 at low stress (linear stress-dependence). This transition takes place between 10 and 40 MPa, depending on porosity. Since the pre-compaction stress required to achieve an aggregate with 25% porosity is not very high, power-law/non-linear creep is not reached for an aggregate with a grain size of  $137 \mu\text{m}$  and the  $n$ -value remains low (see orange curve in Figure 5). However, at lower porosity ( $\ll 5\%$ ), the  $n$ -value at the initial stage of stress relaxation is much higher, around 10. For the sample with a grain size of  $450 \mu\text{m}$  (Figure 6), a similar transition can be observed with  $n$ -values of around 1 at low stress, but the  $n$ -values at high stress are higher and in the range of 3-7 at high and intermediate porosity (5-20%). At a porosity of 1%, the apparent  $n$ -value at the start of relaxation is much higher ( $n$ -value of around 20). However, it must be noted that the relative change in porosity in this phase of the experiment (from 0.9% to 0.1%) is substantial. Hence, the assumption that the porosity remains nearly constant during stress relaxation is no longer valid.

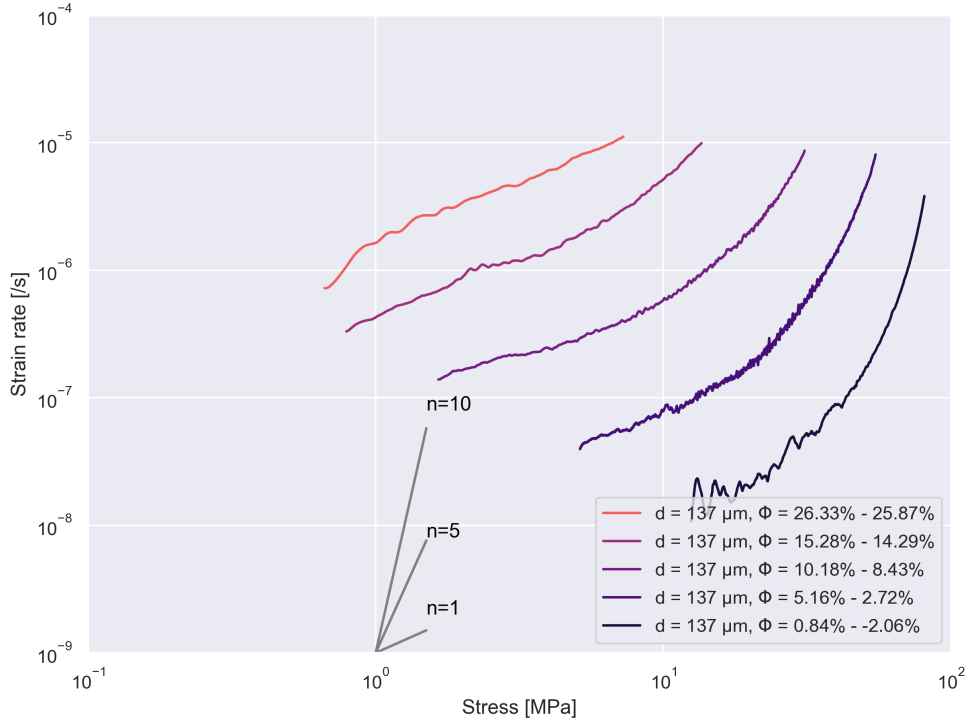


**Figure 5:** Strain rate versus stress data obtained from relaxation experiments on a sample with a grain size of  $137 \mu\text{m}$ , with the pores flooded with saturated brine. Note the change in slope when going from high to low stress and the decrease in strain rates by three orders of magnitude going from high porosity (25%) to low porosity (1%).

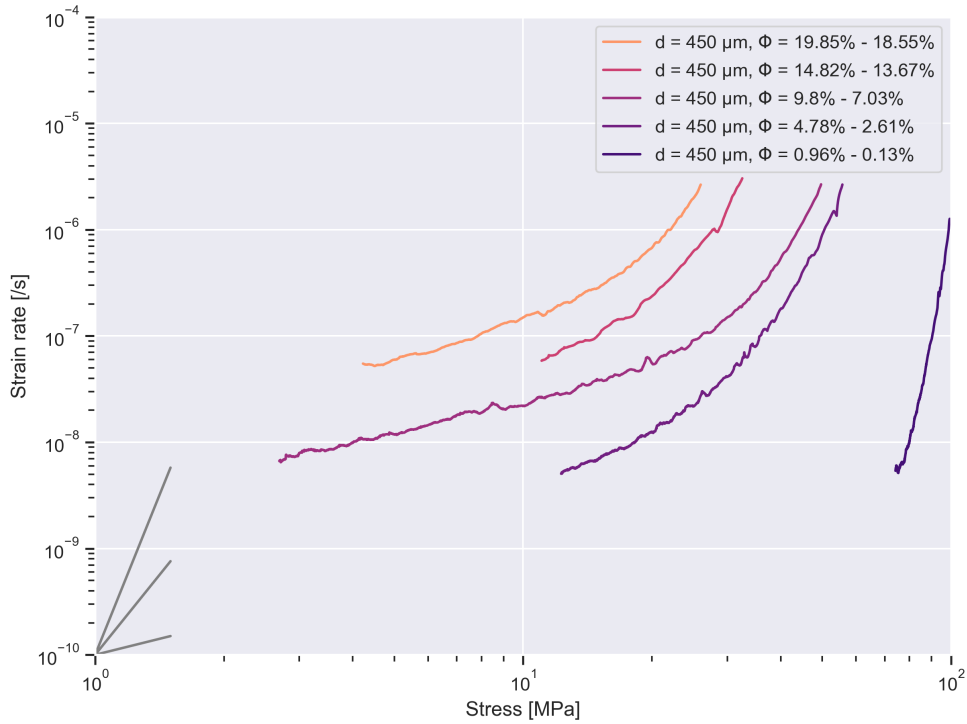


**Figure 6:** Strain rate versus stress data obtained from relaxation experiments on a sample with a grain size of 450  $\mu\text{m}$ , with the pores flooded with saturated brine.

### 3.1.2 Effect of grain size

When the experiments on aggregates with different grain sizes, under brine-saturated conditions, are plotted at equal porosity, the effect of grain size on strain rates is clearly visible (Figure 7-11)). Assuming that the mechanical data can be described with a flow law of the form  $\dot{\epsilon} = A \frac{\sigma^n}{d^m}$ , the grain size dependence ( $m$ ) can be determined (Carter et al. 1993). For a single dominant mechanism operating during compaction, the  $n$ -value and  $m$ -value are constant, such as is the case for pressure solution for which  $n = 1$  and  $m = 3$  (Spiers et al. 1990). Therefore, without any further assumptions, a clear grain size sensitivity ( $m$ -value) can be obtained from the linear creep part, where  $n = 1$  (i.e. at low stress values). At 20% and 10% porosity, the grain size sensitivity is determined to be respectively 2.9 and 3.0 (Figure 7 and 9). At 5% porosity, the grain size sensitivity is reduced and has a value of 2.5 (Figure 10). In the non-linear regime (i.e. at higher stresses), our data suggest that the creep rate is also sensitive to grain size. At a porosity of 15-20%, the grain size dependence is similar to that in the linear regime (Figure 7 and 8), whereas when porosity is below 10% (Figure 9-11) the grain size dependence is certainly lower. Since the variation in  $n$ -values in the non-linear creep part is significant, an exact value for the grain size dependence cannot be determined without any further assumptions.

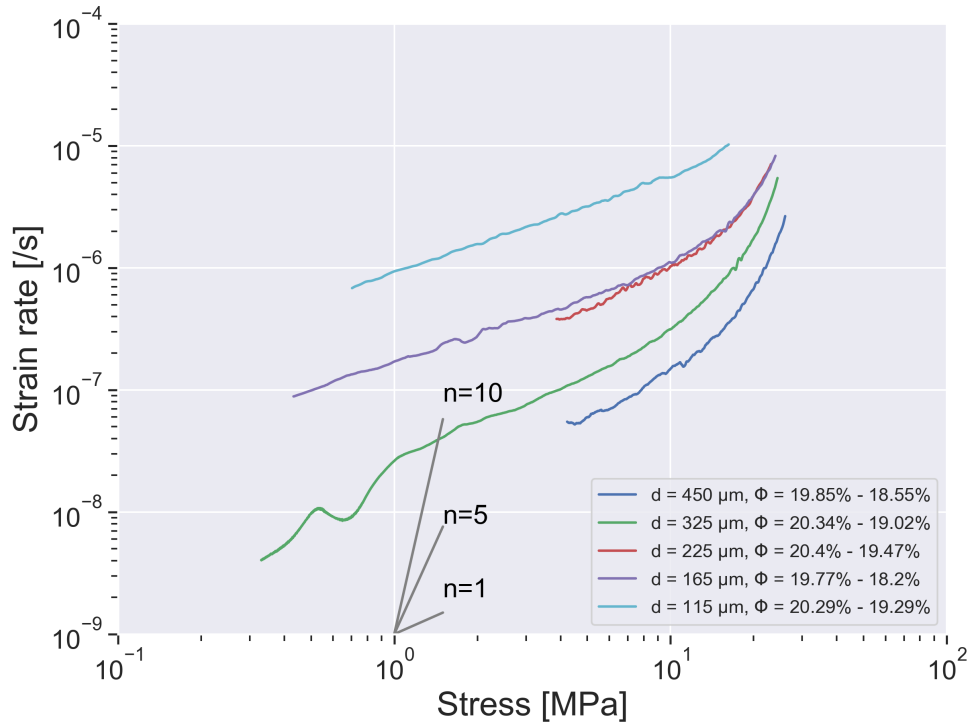


**Figure 7:** Strain rate versus stress data obtained from experiments on aggregates with grain sizes between 115 and 450  $\mu\text{m}$  at 20% porosity, with the pores flooded with saturated brine.

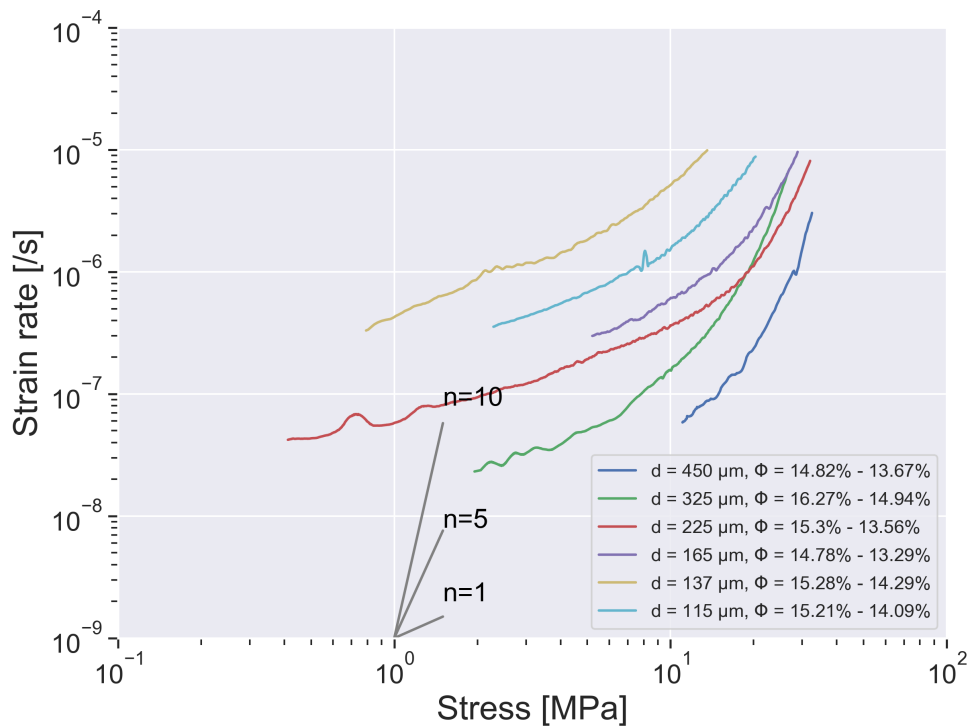


**Figure 8:** Strain rate versus stress data obtained from experiments on grain sizes between 115 and 450  $\mu\text{m}$  at 15% porosity, with the pores flooded with saturated brine.

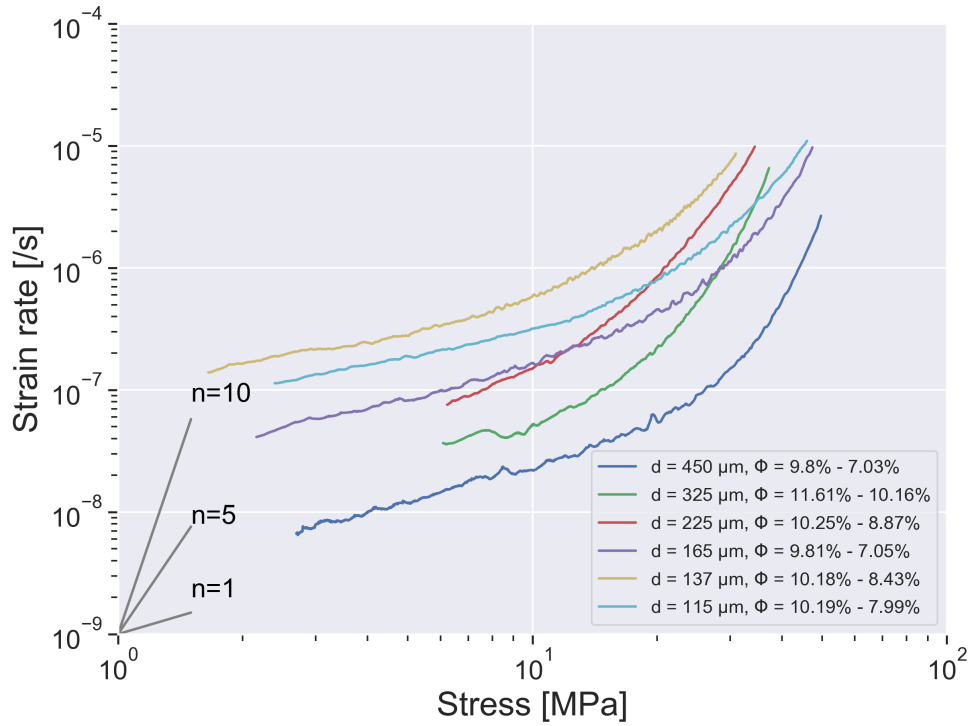


**Figure 9:** Strain rate versus stress data obtained from experiments on grain sizes between 115 and 450  $\mu\text{m}$  at 10% porosity, with the pores flooded with saturated brine.

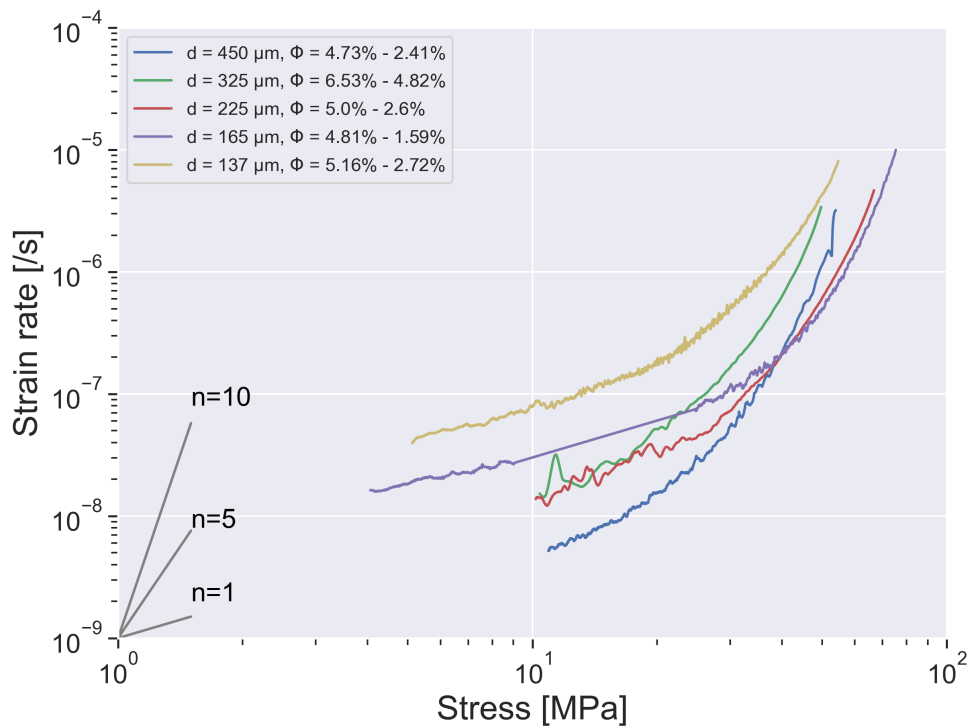


**Figure 10:** Strain rate versus stress data obtained from experiments on grain sizes between 137 and 450  $\mu\text{m}$  at 5% porosity, with the pores flooded with saturated brine.

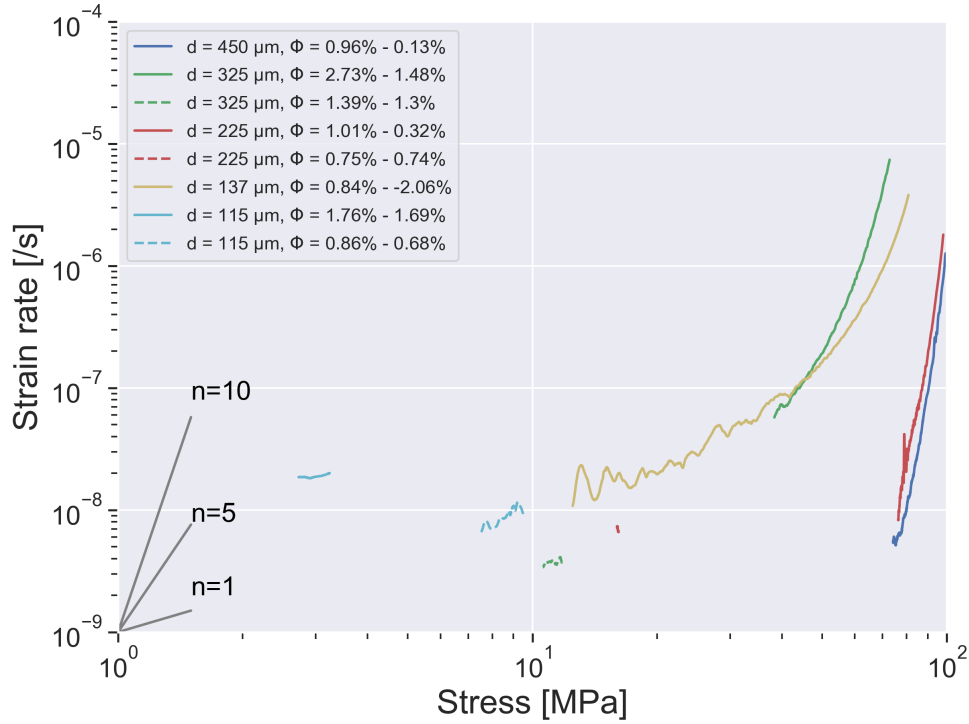


**Figure 11:** Strain rate versus stress data obtained from experiments on grain sizes between 115 and 450  $\mu\text{m}$  at low porosity ( $<2\%$ ), with the pores flooded with saturated brine.

The experimental results obtained at very low porosity ( $<2\%$ ; Figure 11) required very high initial stresses during the pre-compaction stage (up to 100 MPa). As a consequence, during the stress relaxation stages many experiments (especially on coarse-grained material) show a rapid decrease in strain rate, without a sufficient enough drop in stress to reach relevant stress-values ( $<20$  MPa). Hence, obtaining strain rate data at low stress ( $<20$  MPa) in the same relaxation run was not possible. Therefore, during stress relaxation of the samples with 450  $\mu\text{m}$ , 325  $\mu\text{m}$  and 115  $\mu\text{m}$  grain size, the stress was manually reduced and the samples were allowed to continue relaxing at a lower stress. Note that in these experiments, the samples first expanded after reducing the applied stress, prior to relaxation. This process took at least several days and in some cases it was not possible to obtain a steadily decreasing strain rate after a week.

### 3.1.3 Results of experiments on mixtures

The remaining stress relaxation experiments were performed on samples with a distributed grain size as specified in Figure 1. The results of the experiment on Mixture 1 are shown in Figure 12 showing the effect of porosity. Figure 13 shows the results of Mixture 1, 2 and 3, compared to the results of the experiments on single grain sizes of 137  $\mu\text{m}$  and 450  $\mu\text{m}$ , at an aggregate porosity of 5%.

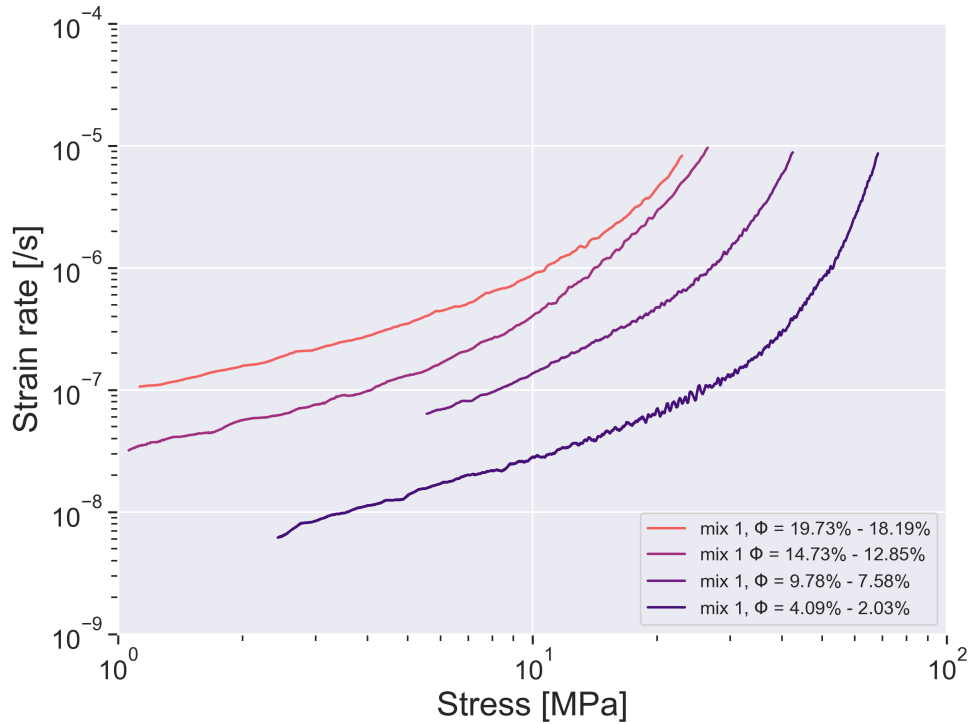


**Figure 12:** Strain rate versus stress data obtained from experiments on Mixture 1, consisting of 50 vol% of  $137 \mu\text{m} \pm 12.5 \mu\text{m}$  grains and 50 vol% of  $450 \mu\text{m} \pm 50 \mu\text{m}$  grains.

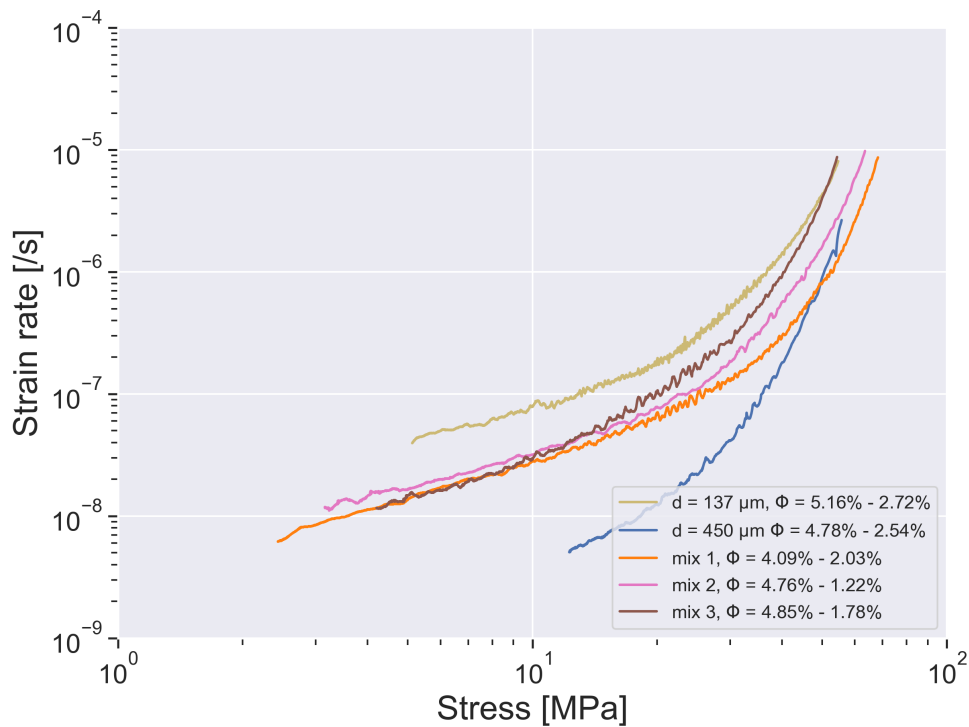


**Figure 13:** Strain rate versus stress data obtained from experiments on aggregates with single grain size fractions of  $137 \mu\text{m}$  and  $450 \mu\text{m}$  and on Mixtures 1, 2 and 3, at an aggregate porosity of 5%.

The results on the mixtures show a similar trend as the behavior of the single grain size fractions with a large stress exponent of 3-6 at high stress and near-linear behavior at low stress. The results of all three mixtures fall within the expected range between the fine ( $137 \mu\text{m}$ ) and coarse ( $450 \mu\text{m}$ ) single grain size fraction. The difference between the three mixtures is not very significant, making it difficult to make

any further statement on how the grain size distribution of each mixture relates to the behavior of its endmember components.

### 3.2 Permeability data

After each of the stress relaxation experiments, the aggregate permeability was measured, as shown in Figure 14. For all experiments, it is clear that the permeability decreases sharply in the low porosity region ( $< 5\%$ ). As the aggregates compact from 25 to 10% porosity, the reduction in permeability is around one order of magnitude. While further compaction from 10% to 1% porosity leads to a drop in permeability by four orders of magnitude. At a porosity of 1% we measured a permeability of  $10^{-17-18} m^2$ . At high porosity  $> 10\%$ , samples with a small grain size (115 and 137  $\mu m$ ) typically have a permeability of up to one order of magnitude lower than the samples with a larger grain size (450  $\mu m$ ) and the mixtures. The intermediate samples with grain sizes of 165  $\mu m$  and 225  $\mu m$  do not clearly fall with this rough trend, but do show permeability values with the range delineated by the finest and coarsest samples. At low porosity, the observed effect of grain size on permeability no longer seems to hold, likely as connectivity has a stronger control on permeability at such low porosity values.

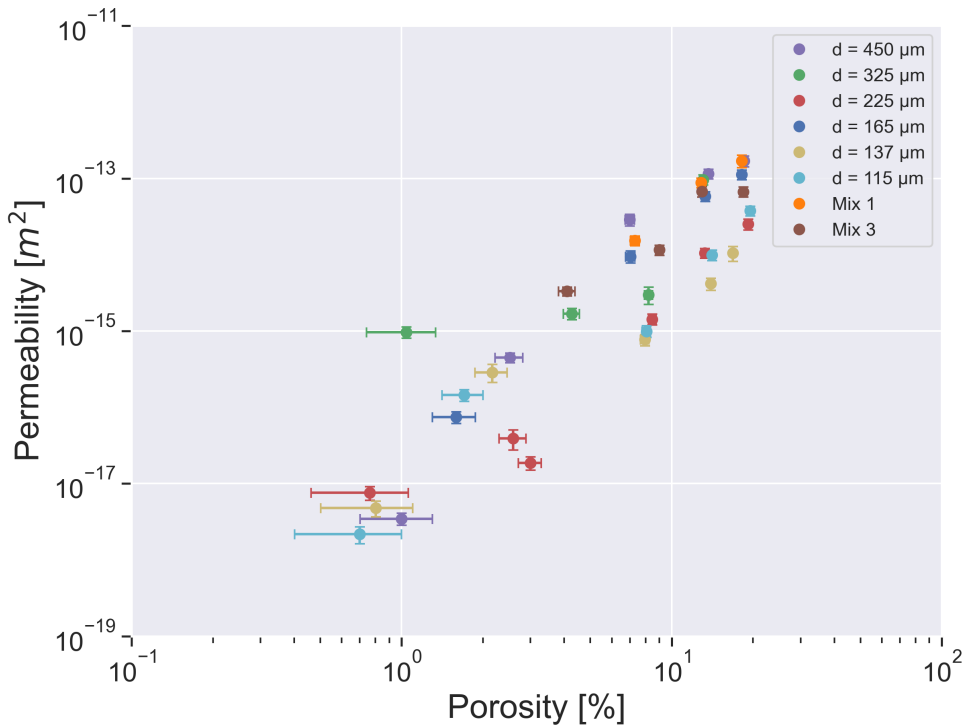


**Figure 14:** Brine permeability versus aggregate porosity for wet compacted granular salt, consisting of either single grain size fractions or mixtures with a distributed grain size.

## 4 Discussion

### 4.1 Deformation mechanisms

As described in the previous section, our data shows a clear effect of porosity, grain size and stress on the creep rate of the sample. The relaxation creep data will not represent steady state flow for a dislocation creep/glide mechanism (Schulze 1984), whereas pressure solution creep is expected to achieve a succession of near-steady state rates as porosity decreases (Spiers et al. 1990). The data can nonetheless be described empirically using a power law of the form (e.g. Bechthold et al. 2004; Zhang et al. 2007; Spiers and Brzesowsky 1993):

$$\dot{\epsilon} = A \exp\left(\frac{-Q}{RT}\right) \cdot \frac{\sigma^n}{d^m} \cdot f(\phi) \quad (5)$$

Here,  $\dot{\epsilon}$  is the compaction strain rate,  $A$  is a material parameter,  $Q$  is the apparent activation energy,  $d$  is the grain size and  $\sigma$  is the applied effective stress.  $n$  and  $m$  are respectively the stress dependence and

grain size dependence.  $f(\phi)$  is a porosity function that describes the effect of porosity on strain rate. In steady state flow, the absolute values of  $Q$ ,  $n$  and  $m$  will depend on the creep mechanism. The value of  $n$  would be exactly 1 for fluid-assisted grain boundary diffusion controlled flow (e.g. pressure solution). For steady state flow by dislocation creep, the value would be in the range of 3-7. Note that, when dislocation mechanisms dominate, the  $n$ -value obtained in stress relaxation experiments is often higher than at steady state (Schulze 1984). Depending on whether creep is due to grain size sensitive (grain boundary) diffusional flow or grain size insensitive dislocation mechanisms, the grain size exponent will be 3 or 0, respectively. In the next sections, we will first look at the mechanical data for the single grain size fraction samples, flooded with saturated brine. Subsequently we will compare the results of the single grain size aggregates with the samples with a distributed grain size (mixtures), before discussing the samples with a different chemical environment and the permeability data.

#### 4.1.1 Deformation mechanism at low stress

In the samples with saturated brine as pore fluid, the  $n$ -values are nearly 1 at stresses less than 10-20 MPa (depending on grain size and porosity, Figure 5 and 6) and a grain size dependence of 2.5-3 is inferred. Classical compaction creep of granular salt by pressure solution is described using a flow law with a stress exponent of 1 and a grain size exponent of 3. Therefore, it is very likely that pressure solution is the dominant mechanism at low stress. This can be described using (Spiers et al. 1990):

$$\dot{\epsilon}_v = A_g V_m \cdot \frac{Z^*}{T} \cdot \frac{\sigma}{d^3} \cdot \frac{1}{e_v^a} \quad (6)$$

in which  $A_g$  is the grain shape packing factor,  $V_m$  is the molar volume ( $m^3 mol^{-1}$ ),  $\sigma$  is the effective stress in Pa and  $d$  is the grain size in  $m$ .  $e_v$  is the volumetric strain defined as  $-\Delta V/V_0$  and  $a$  is shape parameter related to the grain shape.  $Z^*$  represents a phenomenological coefficient defining grain boundary diffusivity ( $m^3 s^{-1}$ ) in terms of the product:

$$Z^* = D \cdot C \cdot S \quad (7)$$

where  $D$  and  $C$  are respectively the diffusivity ( $m^2 s^{-1}$ ) and the concentration ( $m^3/m^3$ ) of the dissolved solid in the grain boundary fluid film.  $S$  is the average thickness of the fluid film ( $m$ ). If we now go back to equation 6, we have a term,  $1/e_v^a$ , that describes the change in strain rate with increasing volumetric strain (i.e. with decreasing porosity), where  $a \approx 2$  when the grains are assumed to be spherical and  $a \approx 4$  when the grains are assumed to be cubic. As such, taking  $a \approx 2$  applies for volumetric strains up to 15% and  $a \approx 4$  to volumetric strains from 15-20% (Schutjens 1991).

Taking an initial aggregate porosity of 40%,  $A_g$  of 22,  $V_m$  of  $2.79 \cdot 10^{-5} m^3 mol^{-1}$ , our experimental data obtained at 25-30% porosity (15-20% volumetric strain) can be fitted to equation 6, assuming a DCS value of  $4 - 8 \cdot 10^{-20} m^3 s^{-1}$ . Spiers et al. (1990) obtained DCS values on the order of  $10^{-19} m^3 s^{-1}$ , whereas direct measurements of thin water film properties of halite under active pressure solution show that DCS is between  $3 \cdot 10^{-20}$  and  $2 \cdot 10^{-18} m^3 s^{-1}$  (De Meer et al. 2002). In similar oedometric stress relaxation experiments by Zhang et al. (2007), a DCS value of  $6 \cdot 10^{-20} m^3 s^{-1}$  was obtained, which is very similar to the value obtained in this study. Hence, we can be quite confident that the same deformation mechanism of pressure solution is operating in our experiments.

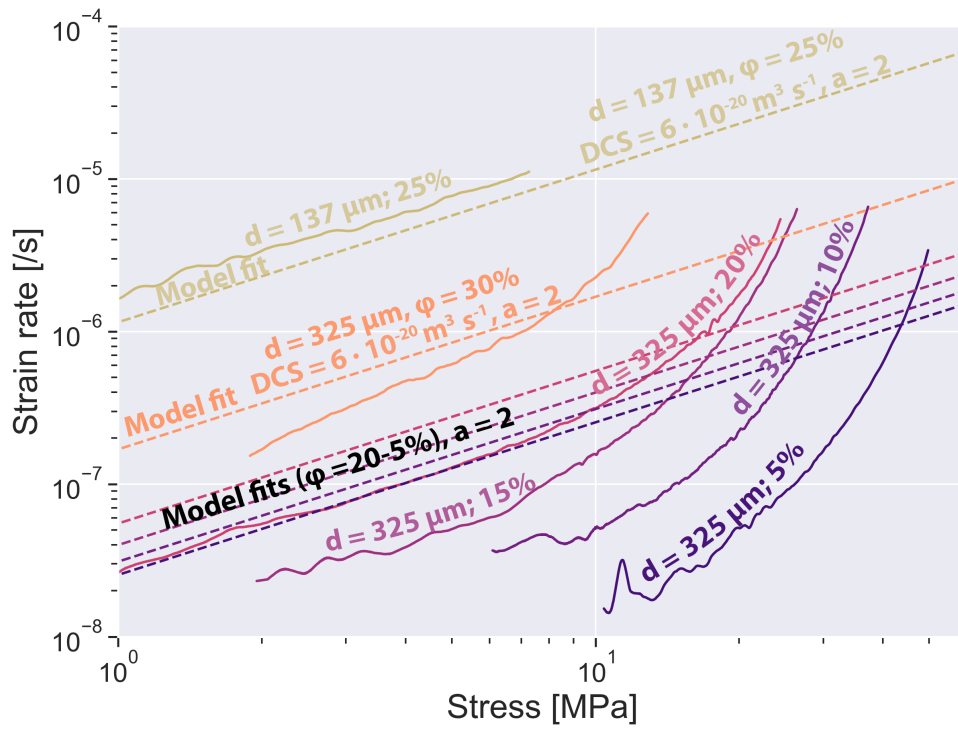


**Figure 15:** Strain rate versus stress data obtained from experiments (solid lines) on samples with a grain size of 137  $\mu\text{m}$  (porosity of 25%) and 325  $\mu\text{m}$  (porosity of 30, 20, 15, 10 and 5%). Dotted lines represent the model fits of the pressure solution model for each of the experiments (corresponding with same color) (Equation 6, with  $a = 2$ ), using a DCS value ( $Z^*$ ) of  $6 \cdot 10^{-20} \text{ m}^3 \text{ s}^{-1}$ . Note that at low porosity (<20%), the model fits predict creep rates of 1-2 orders of magnitude higher than observed in experiments.

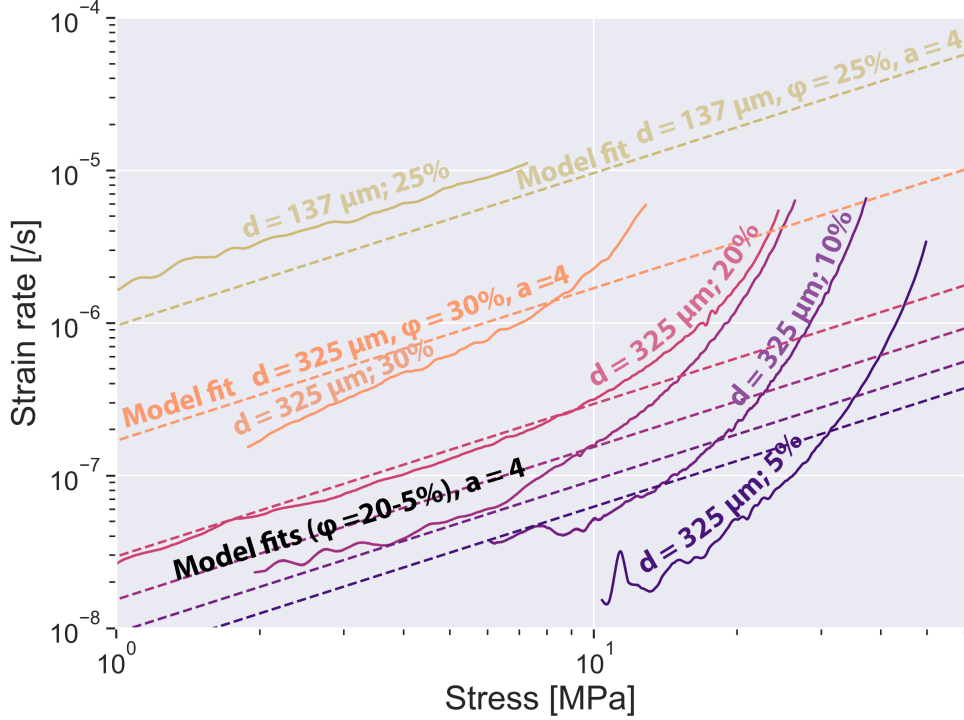


**Figure 16:** Strain rate versus stress data obtained from experiments (solid lines) on samples with a grain size of 137  $\mu\text{m}$  (porosity of 25%) and 325  $\mu\text{m}$  (porosity of 30, 20, 15, 10 and 5%). Dotted lines represent the model fits of the pressure solution model for each of the experiments (corresponding with same color) (Equation 6, with  $a = 4$ ), using a DCS value ( $Z^*$ ) of  $6 \cdot 10^{-20} \text{ m}^3 \text{ s}^{-1}$ . Note that the cubic volumetric strain equation overestimates strain rates at low porosity by 0.5-1 order of magnitude.

#### 4.1.2 Required adjustments to pressure solution creep model

The classical theory for compaction creep by pressure solution has been determined at high porosity/small volumetric strains (>30-40% porosity). Therefore, the evolution of the grain shape with porosity change can be quite well described using a numerical solution for spheres or cubes (Schutjens 1991). However, including this type of grain size evolution through  $1/e_v^{2-4}$  results in an overestimation of the strain rates at low porosity (<20%). We have also tried to use other porosity functions (e.g. Pluymakers and Spiers 2015; Korthaus 1998). However, all of these functions resulted in an overestimation of the creep rates at low porosity. Therefore, we have obtained an empirical function based on the dataset obtained in this study that provides a better fit of the effect of porosity on strain rates. This function is given by:

$$f_1(\phi) = 4.09 \cdot 10^{-3} \cdot \phi^{2.594} \quad (8)$$

using this equation we can now rewrite equation 6, such that:

$$\dot{\epsilon}_v = \frac{A_{ps}}{T} \cdot \frac{\sigma}{d^3} \cdot f_1(\phi) \quad (9)$$

Note that  $A_{ps}(\text{m}^3 \text{K}^{-1} \text{MPa}^{-1} \text{s}^{-1})$  in this equation is a material parameter that no longer has a micro-physical basis and takes the value of  $3.61 \cdot 10^{-17}$  at a temperature of 301 K (where these results were obtained). Recognizing that it is expected to exhibit an Arrhenius dependence on temperature it can be rewritten into:

$$\dot{\epsilon}_{ps} = \frac{A_{ps0} \exp\left(\frac{-\Delta H}{RT}\right)}{T} \cdot \frac{\sigma}{d^3} \cdot f_1(\phi) \quad (10)$$

Where  $\Delta H$  is the activation energy for grain boundary diffusion as determined by Spiers et al. (1990), which takes the value of  $-24530 \text{ J mol}^{-1}$ . Hence the pre-exponential material parameter ( $A_{ps0}$ ) takes the value of  $6.12 \cdot 10^{-13} \text{ m}^3 \text{K}^{-1} \text{MPa}^{-1} \text{s}^{-1}$ . The overestimation of strain rates at low porosity using either theoretical porosity functions (e.g. Spiers et al. 1990; Pluymakers and Spiers 2015) or empirical functions obtained at high porosity (e.g. Korthaus 1998) has been observed in recent experiments on

compaction creep in aggregates at low porosity (Zhang et al. 2007; Kröhn et al. 2012). Analysis of the experimental data obtained by Zhang et al. (2007) in the same porosity range results in a very similar empirical porosity function as the one obtained from this study. This indicates that: (1) the porosity dependence obtained at high porosity cannot be extrapolated to lower porosity and would result in underestimating timescales for sealing of a repository, and (2) simple assumptions on the evolution of contact area and contact stresses break down at low porosity.

It is important to emphasize here that the stress state of the sample in the configuration used in this study is likely not isotropic as the apparatus is a 1D oedometer. Therefore, discrepancies can exist between the work done in this study and Zhang et al. (2007), and earlier work done by Spiers et al. (1990) and Schutjens (1991) on 3D compaction with different boundary conditions. Hence, this may result in apparent differences in the inferred DCS value.

#### 4.1.3 Deformation mechanism at high stress

In all samples flooded with saturated brine a transition occurred to non-linear creep at stresses above 10-20 MPa, with  $n$ -values in the range 2-7, except for at low porosity where apparent  $n$ -values of 10-20 were obtained. This is similar to  $n$ -values found in constant stress experiments on crushed rock salt that indicate stress exponents of 3-7 (Korthaus 1998) and to  $n$ -values found in many experiments on dense rock salt at intermediate stress levels (Hunsche and Hampel 1999; Carter et al. 1993). In dense rock salt this is generally attributed to dislocation climb processes. For crushed rock salt the exact mechanism has not been identified and in general is fitted using a power law with an exponent of 5 (Korthaus 1998; Callahan et al. 1998). The variation in stress exponent makes it challenging to obtain a grain size dependence, but there is clear evidence for some dependence on grain size, which ranges from 0 to 2. Hence, true dislocation climb alone cannot describe what goes on in this regime. Another candidate for compaction creep at moderately high stresses ( $< 20$  MPa) is caused by plasticity coupled dissolution of grain contacts (Spiers and Brzesowsky 1993). This mechanism may describe the grain size dependence shown in the non-linear field, but at present no model exist to account for this.

Although the variation in the slope of the strain rate-stress curves is considered to be too large to be explained by one single mechanism, we nevertheless use the BGR compaction creep law with an  $n$ -value of 5 as our starting point to empirically describe the behavior at high stresses. For the present aim, this can be justified as the coupled model (section 4.5) will show that the mean stress in the backfill will remain within the domain where linear creep dominates, unless the grain size of the backfill will be very coarse ( $> 2$ mm). Therefore, the non-linear creep regime can be almost entirely neglected, which means that extrapolation to higher stress values is likely not necessary. The BGR law for compaction creep is given as:

$$\dot{\epsilon}_{\text{dis}} = A_{\text{BGR}} \exp\left(\frac{-Q_{\text{BGR}}}{RT}\right) \cdot \bar{\sigma}^5 \cdot f_{\text{BGR}}(\phi) \quad (11)$$

where  $A_{\text{BGR}}$  is a material parameter ( $1.09 \cdot 10^{-6} \text{ s}^{-1} \text{ MPa}^{-5}$ ),  $Q_{\text{BGR}}$  is the activation energy ( $54000 \text{ J mol}^{-1}$ ),  $\bar{\sigma}$  is the mean stress and  $f_{\text{BGR}}(\phi)$  is an empirical porosity function given by:

$$f_{\text{BGR}}(\phi) = \left[ \frac{0.01648}{(0.0003 - \frac{1}{\phi_0^{0.1}} + \frac{1}{\phi^{0.1}})^{2.25}} \right]^{3/5} \quad (12)$$

where  $\phi_0$  is the initial porosity. Although Equation 12, is able to describe the effect of porosity on creep rates down to around 10%, it overestimates creep rates at lower porosity. Hence, we use the same approach as for the pressure solution creep domain and use a porosity function that is able to fit the creep rates observed in the experiments at low porosity, given by:

$$f_2(\phi) = 1.99 \cdot 10^{-3} \cdot \phi^{3.699} \quad (13)$$

By replacing  $f_{\text{BGR}}(\phi)$  with  $f_2(\phi)$  in Equation 11, we obtain a function that is in agreement with the experimental data in the non-linear domain for a coarse grain size of 450  $\mu\text{m}$ . However, the absence of any grain size dependence underestimates compaction rates for the smaller grain size aggregates. As a well developed mechanistic based model does not exist for this type of behavior, we have to use an empirical function that allows for the grain size sensitivity observed in this study. The non-linear creep data in this study is best described using a grain size sensitivity of 1.8. Hence, we can describe the high stress data using:

$$\dot{\epsilon}_{\text{nlc}} = \frac{A_{\text{nlc}}}{d^{1.8}} \exp\left(\frac{-Q_{\text{BGR}}}{RT}\right) \cdot \bar{\sigma}^5 \cdot f_2(\phi) \quad (14)$$

in which  $A_{\text{nlc}}$  takes the value of  $1.03 \cdot 10^{-12} \text{ m}^{1.8} \text{ MPa}^{-1} \text{ s}^{-1}$  and  $\frac{A_{\text{nlc}}}{d^{1.8}}$  is equal to  $A_{\text{BGR}}$  for a grain size of  $450 \text{ }\mu\text{m}$ . The apparent high stress sensitivity combined with the presence of grain size sensitivity may indicate that a coupling between grain contact dissolution and dislocation creep is controlling creep rates at these conditions. In future, our aim is to develop a mechanistic based model that allows extrapolation of the results obtained at high stresses and the deformation mechanisms controlling the rates at these conditions.

## 4.2 A composite flow law for backfill compaction

We have modified both the pressure solution compaction creep law and the BGR creep law for compaction by dislocation creep to account for the decrease in strain rates at low porosity. Recognizing that pressure solution creep and dislocation creep are independent mechanisms that work in parallel, we consider that the total creep rate can be described by the sum of the two, giving the composite flow law:

$$\dot{\epsilon} = \dot{\epsilon}_{\text{dis}} + \dot{\epsilon}_{\text{ps}} \quad (15)$$

Since pressure solution creep is proportional to  $\sigma$  and dislocation creep is proportional to  $\sigma$  to the power 5, pressure solution creep will be dominant in the low stress region and dislocation creep in the high stress region. Predictions made by this composite compaction model are presented in Figures 17 - 19, for respectively a grain size of  $137 \text{ }\mu\text{m}$  and  $450 \text{ }\mu\text{m}$  and for the entire range of tested grain sizes at a fixed porosity of  $10\%$ .

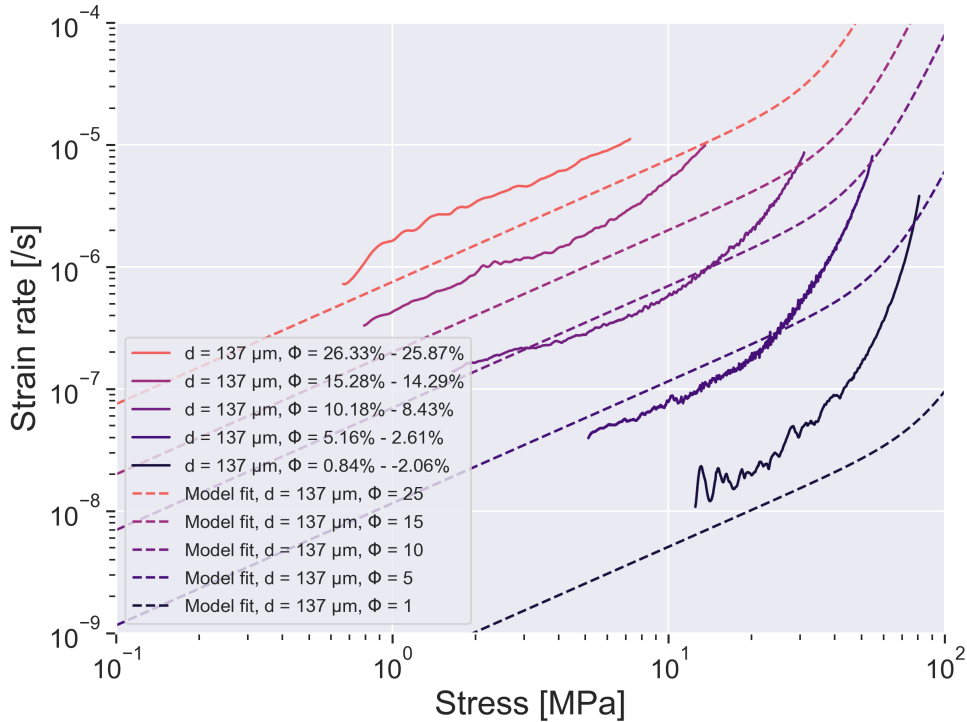


**Figure 17:** Strain rate versus stress data obtained from relaxation experiments on a sample with a grain size of  $137 \text{ }\mu\text{m}$ , including the strain rates predicted by the composite compaction model (Equation 15). Note that the model has a reasonable fit in the low stress/pressure solution domain, but does not predict the transition to the non-linear creep at the right stresses, due to not taking the grain size dependence into account.

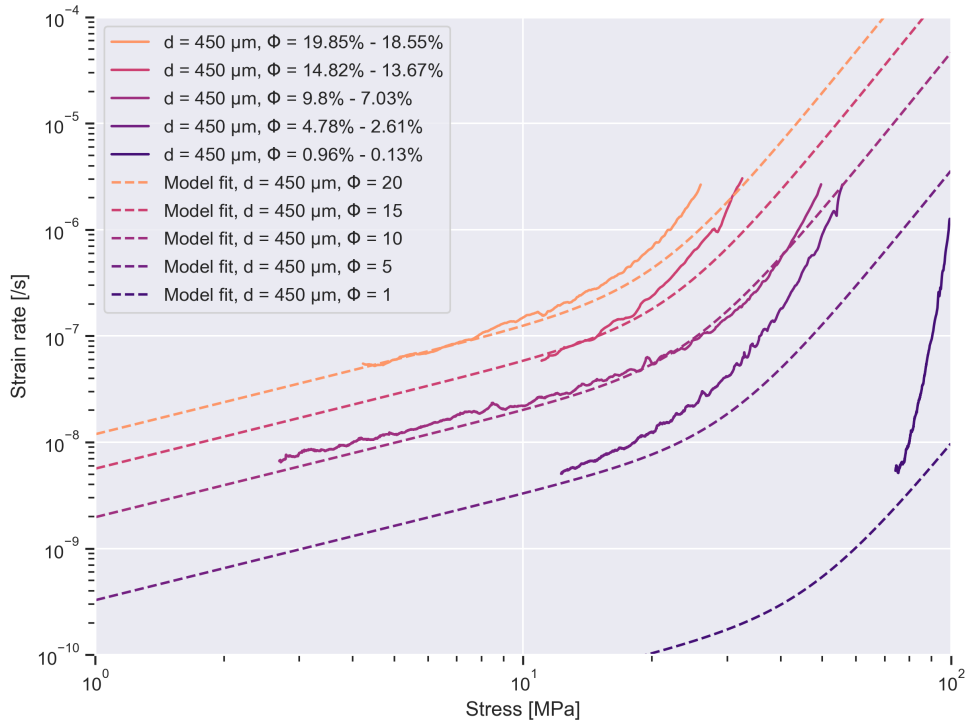


**Figure 18:** Strain rate versus stress data obtained from relaxation experiments on a sample with a grain size of  $450\ \mu\text{m}$ , including the strain rates predicted by the composite compaction model (Equation 15). Note that in contrast to Figure 17, the transition to the non-linear creep is predicted at the right stress in the coarse grain size.

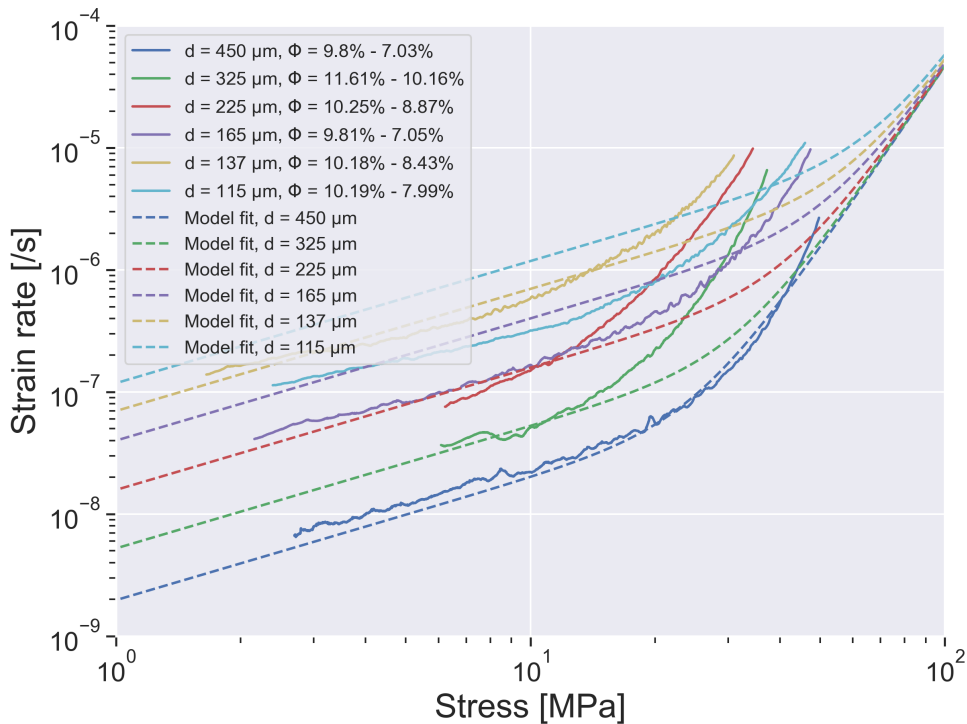


**Figure 19:** Strain rate versus stress data obtained from relaxation experiments at a porosity of 10%, including the strain rates predicted by the composite compaction model (Equation 15). Note the misfit in the non-linear domain due to the absence of grain size dependence.

The results of the composite model for compaction creep (Equation 15) show good agreement with the

experimental data at low stress (in the domain where pressure solution is dominant), for a wide range of grain sizes, stresses and porosity in. At high stresses, the BGR model for compaction creep is able to describe the strain rates in the coarse grained material (450  $\mu\text{m}$ , see Figure 18). However, in the samples with a smaller grain size (Figure 17 and 19), the high-stress, BGR model branch of the composite flow law underestimates the strain rate by up to one order of magnitude. Therefore, we have developed an empirical function (Equation 14) to account for the grain size sensitivity in the non-linear creep domain at high stress. Using

$$\dot{\epsilon} = \dot{\epsilon}_{\text{nlc}} + \dot{\epsilon}_{\text{ps}} \quad (16)$$

we can now obtain a better agreement with our experimental results. The results of this modified composite compaction model are presented in Figures 20-22.

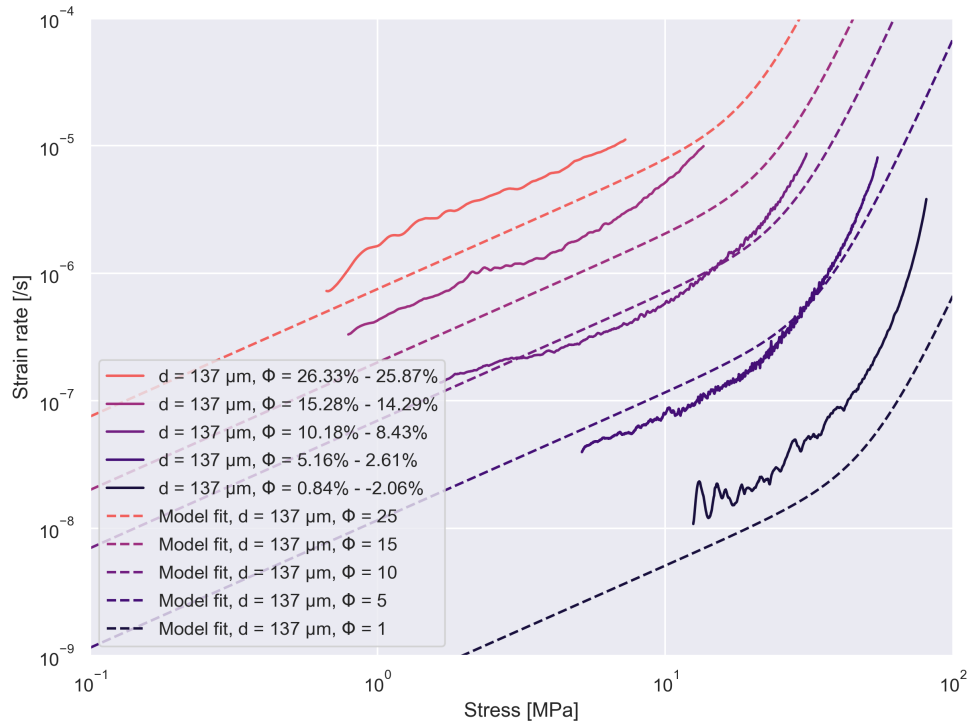


**Figure 20:** Strain rate versus stress data obtained from relaxation experiments on a sample with a grain size of 137  $\mu\text{m}$ , including the strain rate predicted by the modified composite compaction model (Equation 16).

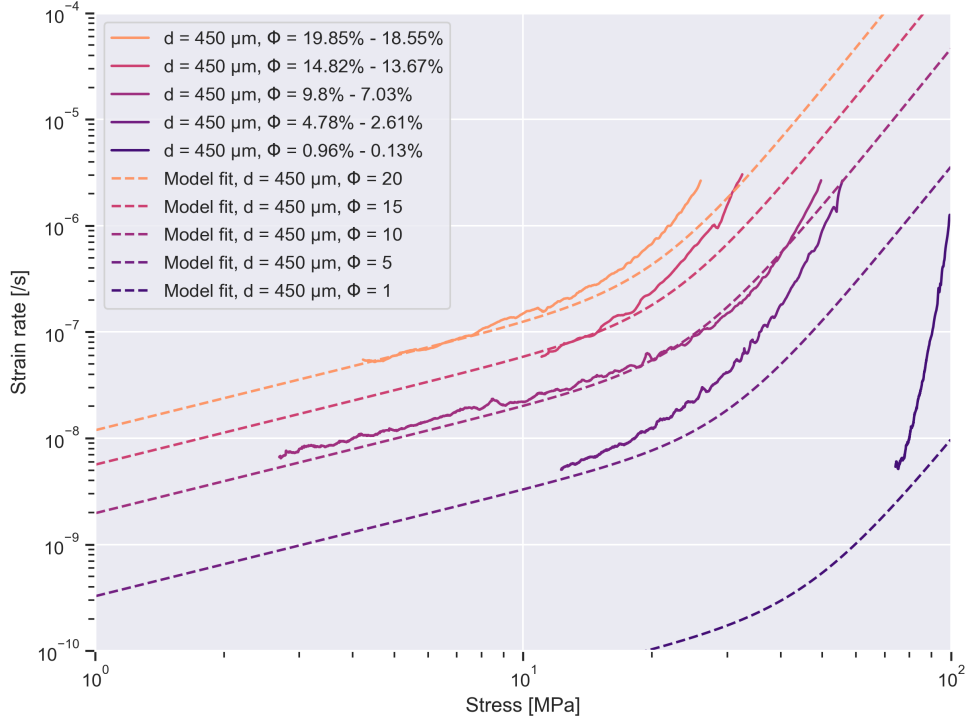


**Figure 21:** Strain rate versus stress data obtained from relaxation experiments on a sample with a grain size of  $450 \mu\text{m}$ , including the strain rate predicted by the modified composite compaction model (Equation 16).

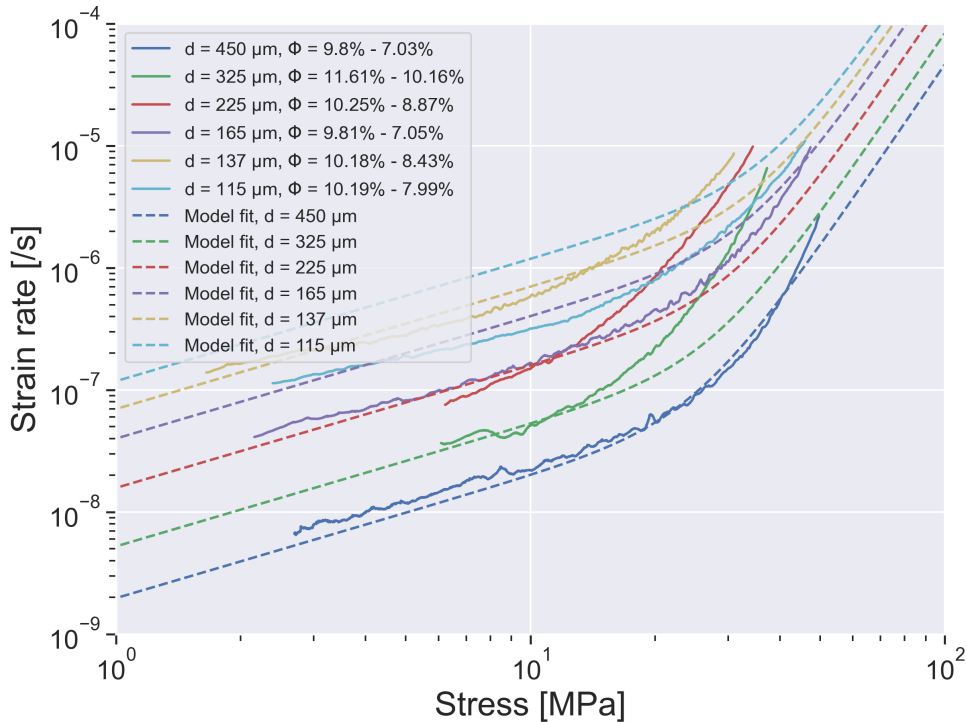


**Figure 22:** Strain rate versus stress data obtained from relaxation experiments at a porosity of 10%, including the strain rate predicted by the modified composite compaction model (Equation 16).

We can now use the modified composite compaction model to obtain a deformation mechanism map that describes under which conditions pressure solution creep or non-linear creep is dominant. Equation 16 can be rewritten such that we can evaluate where  $\dot{\epsilon}_{nlc} = \dot{\epsilon}_{ps}$  as a function of stress, grain size and

porosity for compaction creep under brine-saturated conditions. The result of this is shown in Figure 23.

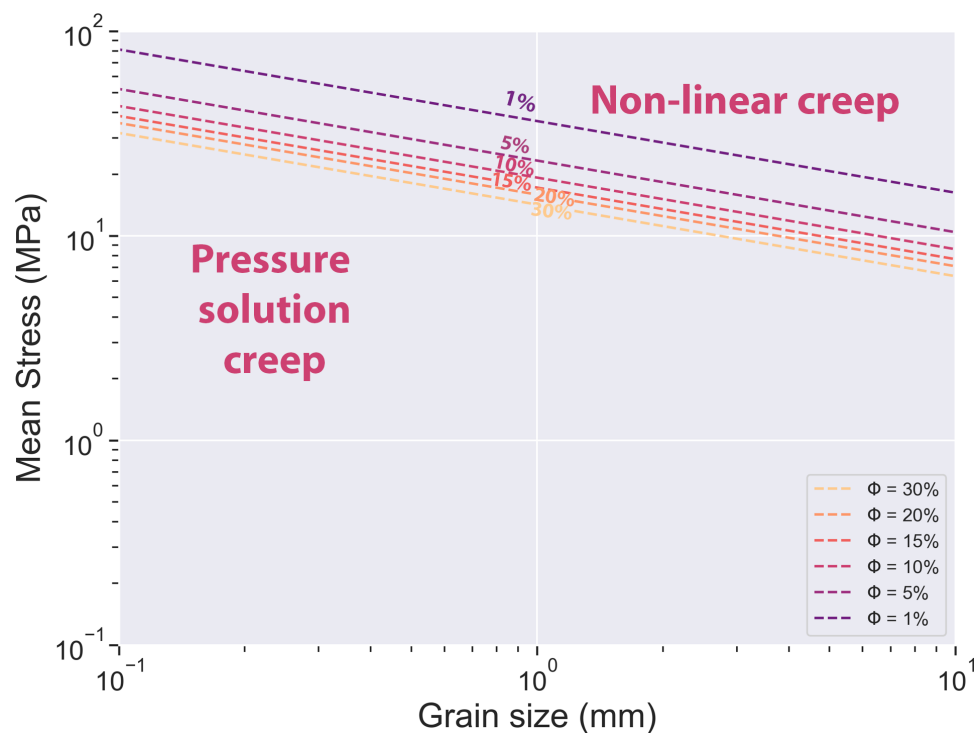


**Figure 23:** Deformation mechanism map for compaction creep in granular salt in log stress versus log grain size space for a porosity of 1-30%, based on Equations 14, 10 and 16. Note that for a grain size of 500  $\mu\text{m}$ , a transition from pressure solution to non-linear creep is expected between 15 MPa (at 30% porosity) and 50 MPa (1% porosity).

For a backfilled repository at a depth of 700-800 m, a lithostatic pressure of around 15 MPa can be expected. Hence the maximum stress to which the backfill will be subjected will be around 15 MPa. Figure 23 shows that for grain sizes smaller than 0.5 mm, compaction is only expected to occur within the pressure solution (linear) creep domain. For backfill with larger grain sizes, we have to consider that non-linear creep can occur during compaction of the backfilled gallery.

### 4.3 Compaction creep in mixtures with a distributed grain size

So far we have considered the results of our compaction creep experiments obtained for aggregates with a single grain size (e.g. a grain sizes fraction with a very narrow range of  $\pm 12\text{-}50 \mu\text{m}$ ). For a real repository it is expected that the crushed rock salt used to fill the repository consist of material obtained from the excavation of the repository itself. Hence, the grain size will be determined by the method used to excavate the repository and/or whether additional treatment is performed to further reduce the grain size or optimize the mixture. Without any special treatment the grain size distribution is expected to have a much wider range. Even with further treatment, the variation in grain size is expected to be larger than used in the single grain size experiments in this study (i.e.  $> 0.05 \text{ mm}$  variation in grain size). For this reason, many previous studies on crushed rock salt have been performed on crushed rock salt with a distributed grain size. Because of the recognized dependency of creep rates on grain size, many of these mixtures have a predetermined, known grain size distribution in order to be able to compare results between different laboratories (e.g. Kompass or Deborah backfill mixture; Kröhn et al. 2012; Czaikowski et al. 2012) However, for such a mixture with a wide distribution, the contribution of individual grain size fractions to the overall strain rate is unknown and may vary depending on porosity.

Compaction creep experiments on aggregates with a single grain size below 0.5 mm (e.g. this study Spiers et al. 1990; Spiers and Brzesowsky 1993; Zhang et al. 2007) show a very clear and strong dependence on grain size, with rates increasing for finer-grained aggregates ( $\dot{\epsilon} \propto d^{-3}$ ). Nevertheless, previous models for compaction of mixtures use a single grain size as input parameter (Bechthold et al. 2004; Callahan et al. 1998), by simply taking an average grain size to represent the mixture, or by treating grain size as

a fitting parameter such that the models fit the rates observed in lab experiments. However, this makes extrapolation beyond laboratory conditions questionable and relies on using the exact same backfill grain size distribution in the repository to allow for extrapolation of the lab data. Hence a key aim of the experiments on mixtures containing different grain size fractions is to compare the compaction rates of mixtures with those of single grain size fractions. This is done to subsequently test if the compaction rate of a mixture of grain size fractions can be predicted from the rates of single grain size fractions.

#### 4.3.1 A model for compaction creep in mixtures: theory

The present compaction creep tests on granular salt aggregates composed of single grain size fractions indicate that two distinct regimes can be recognized: a linear regime, which is considered to be governed by pressure solution creep, and a non-linear regime, which is attributed to dislocation creep (e.g. see Figure 20). Since there are some uncertainties on the grain size dependence in the non-linear domain, we focus on the pressure solution (linear) domain of the results. For a single grain size fraction, compaction creep by pressure solution can be described using Equation 10, in which the applied stress on the sample is related to the measured strain rate at the scale of the sample (i.e. the bulk strain rate). If we now consider an idealized sample containing a range of grain sizes (see Figure 24), then following Equation 10, we can calculate the strain rate for a given applied stress for each grain size fraction. This would result in smaller grains deforming at a higher strain rate than larger grains. However, this would inherently result in heterogeneous strain rates throughout the sample. Conversely, when the grains in the sample are each subjected to the same, constant strain rate, this will result in heterogeneous stresses throughout the sample. Hence this leads to two end-member models with either uniform stress or uniform strain rate throughout the compacting sample (Ter Heege et al. 2004).

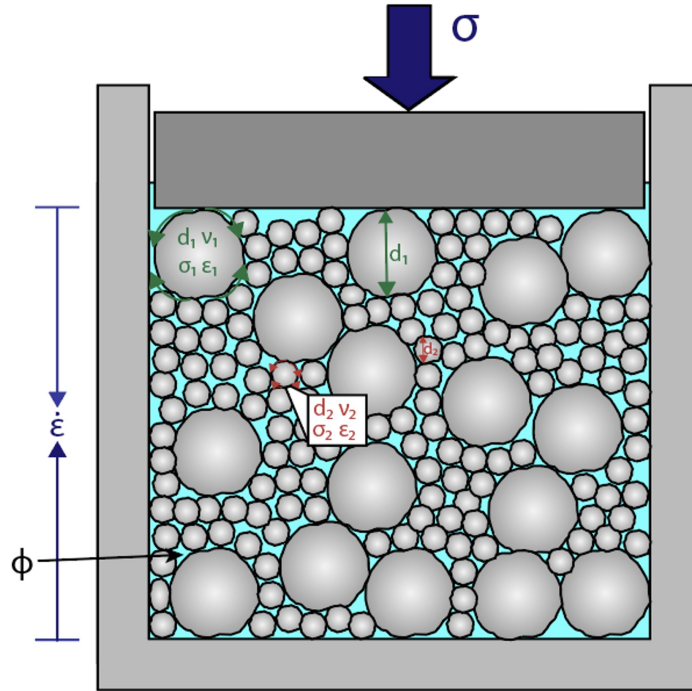


**Figure 24:** Schematic representation of a sample with a distributed grain size, having porosity  $\phi$ , subjected to 1D compaction under an applied stress  $\sigma$  deforming at a sample-scale (bulk) strain rate  $\dot{\epsilon}$ . In this figure, the sample has a bi-modal distribution comparable to Mixture 1, with two grain size fractions  $d_1$  and  $d_2$ , each having a volume fraction of 0.5 ( $\nu_1$  and  $\nu_2$ , respectively). Assuming homogeneous stress ( $\sigma_1 = \sigma_2$ ), the strain rates ( $\dot{\epsilon}_1$  and  $\dot{\epsilon}_2$ ) can be calculated. Conversely when homogeneous strain rate is assumed,  $\sigma_1$  and  $\sigma_2$  can be calculated, assuming  $\dot{\epsilon}_1 = \dot{\epsilon}_2$ . Note that the subscript do not refer to the principal stress/strain axes, but the vertical components of stress/strain rate for each grain size fraction.

If the stress is assumed to be uniform throughout an aggregate with a distributed grain size, then each grain size fraction will deform at a different rate. Assuming that the contribution of each grain size

fraction is determined by its volume fraction within the aggregate, the strain rate can be calculated such that

$$\dot{\epsilon}_{\text{tot}} = \sum_{i=1}^{i=j} \dot{\epsilon}_i \nu_i \quad (17)$$

in which  $\dot{\epsilon}_i$  is the strain rate calculated for an individual grain size fraction using Equation 10 and  $\nu_i$  is the volume fraction occupied by that grain size fraction as a fraction of the total solid phase present. Note that the probability of our mixtures (Figure 1) divided by the total probability gives the volume fractions. Assuming uniform stress throughout the aggregate can be considered the upper bound for predicting the compaction rate in a mixture, as all grains can deform at their theoretical maximum strain rate for a given applied stress. If instead the strain rate is assumed to be uniform throughout the material, the stress on each grain size fraction can be calculated using:

$$\sigma_{\text{tot}} = \sum_{i=1}^{i=j} \sigma_i \nu_i \quad (18)$$

where now  $\sigma_i$  can be obtained from rewriting Equation 10 in terms of stress as a function of strain rate. This can be considered as the lower bound prediction for the strain rate of a mixture, as the grains all will be subjected to the stress required to achieve a specific strain rate, which may be less than the maximum stress imposed in the uniform-stress scenario. Note, that this assumes that the porosity function (Equation 8) is not affected by the aggregate having a distributed grain size. For these models, it is also assumed that grain size is spatially non-correlated, i.e. no weak layers of fine grains or load-bearing frameworks of large grains are formed (Ter Heege et al. 2004).

### 4.3.2 A model for compaction creep in mixtures: results

We have developed two models that predict the upper and lower bound compaction rates for creep behavior of a granular salt mixture with a known grain size distribution. Using these models, we can determine the upper and lower boundary creep rates for each of the grain size mixtures tested in our experiments. The results of these models compared to the experimental results of the mixtures are shown in Figure 25 and 26 for Mixture 1 at respectively 20 and 5% porosity, and for Mixture 2 and 3, at 5% porosity (Figure 27 and 28).

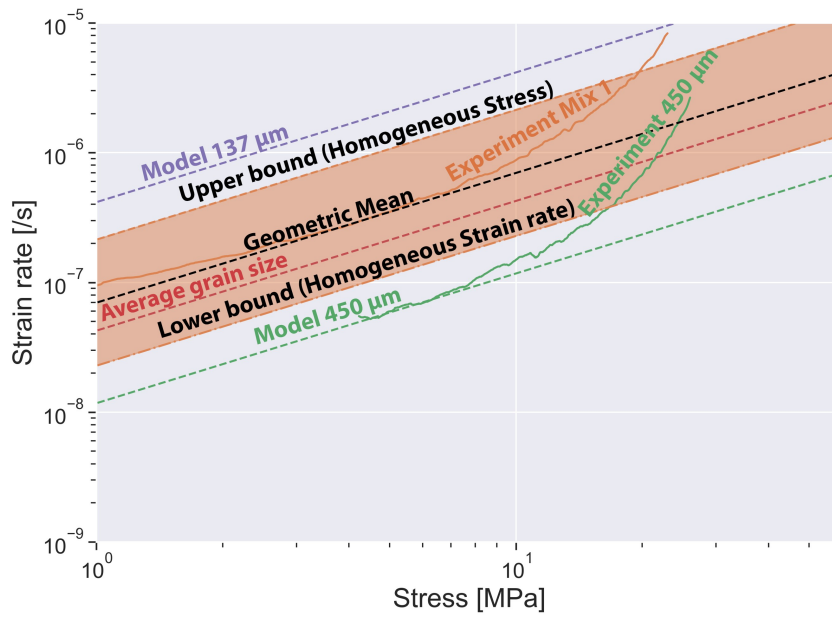


**Figure 25:** Strain rate versus stress of the experiments on Mixture 1 and an aggregate with a single grain size fraction of 450  $\mu\text{m}$  at 20% porosity (solid lines). Dashed lines represent the model results for the predicted pressure solution creep rates in an aggregate with a single grain size fraction of 137  $\mu\text{m}$  or 450  $\mu\text{m}$ , and the upper and lower bound compaction rates of Mixture 1 based on the model for compaction creep in a mixture by pressure solution.

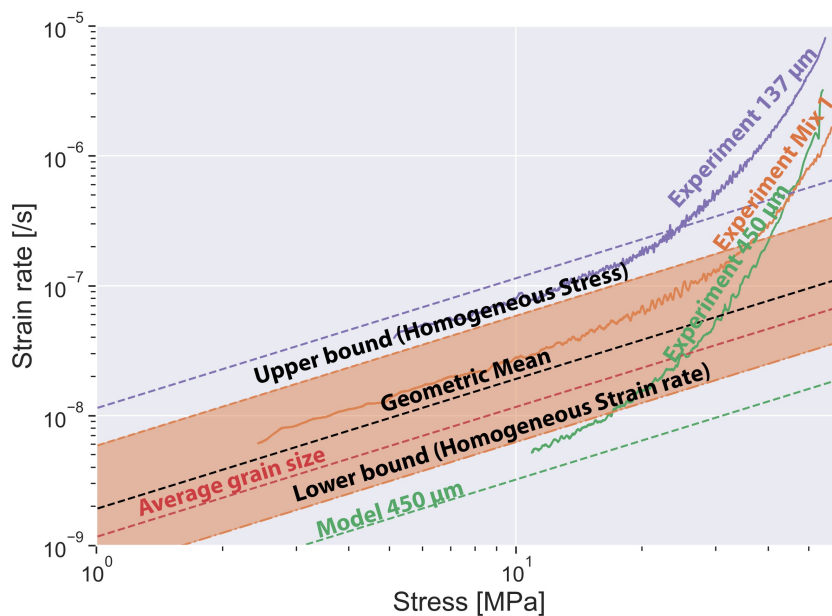


**Figure 26:** Strain rate versus stress of the experiments on Mixture 1 and an aggregate with a single grain size fraction of 137 and 450  $\mu\text{m}$  at 5% porosity (solid lines). Dashed lines represent the model results for the predicted pressure solution creep rates in aggregates with single grain size fractions of 137  $\mu\text{m}$  or 450  $\mu\text{m}$ , and the upper and lower bound compaction rates of Mixture 1 based on the model for compaction creep in a mixture by pressure solution.

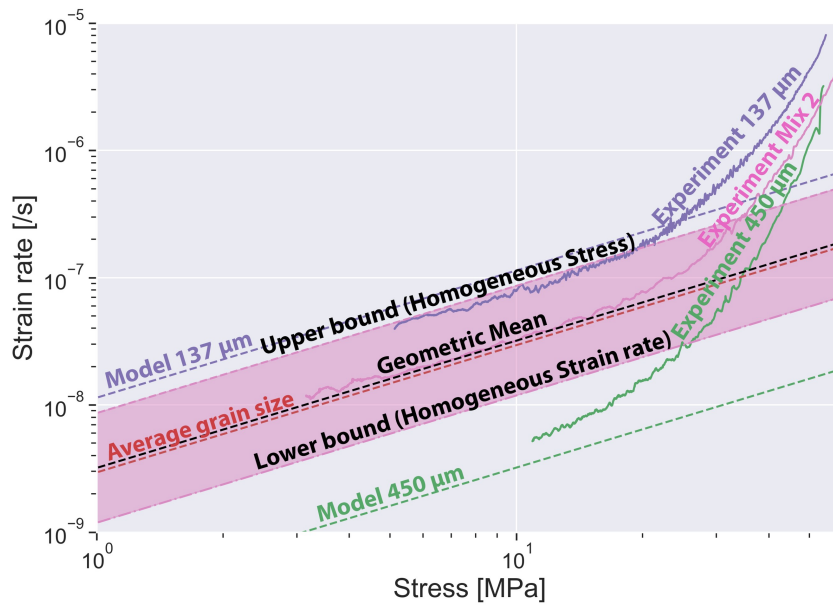


**Figure 27:** Strain rate versus stress of the experiment on Mixture 2 and an aggregate with a single grain size fraction of 137 or 450  $\mu\text{m}$  at 5% porosity (solid lines). Dashed lines represent the model results for the predicted pressure solution creep rates in aggregates with a single grain size fraction of 137  $\mu\text{m}$  or 450  $\mu\text{m}$ , and the upper and lower bound compaction rates of Mixture 2 based on the model for compaction creep in a mixture by pressure solution.

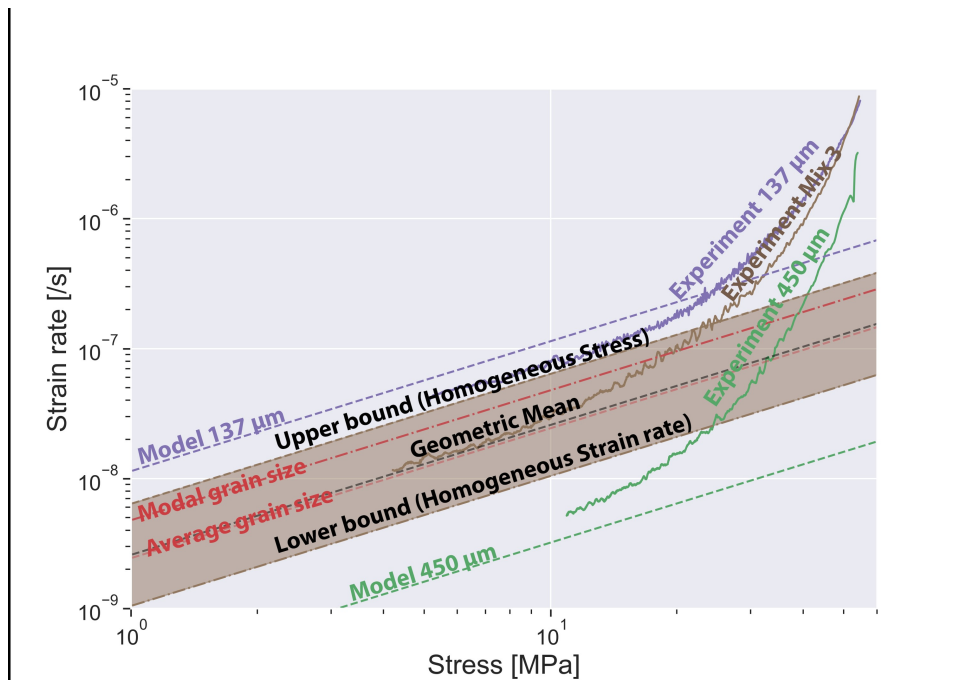


**Figure 28:** Strain rate versus stress of the experiment on Mixture 2 and an aggregate with a single grain size fraction of 137 or 450  $\mu\text{m}$  at 5% porosity (solid lines). Dashed lines represent the model results for the predicted pressure solution creep rates in aggregates with a single grain size fraction of 137  $\mu\text{m}$  or 450  $\mu\text{m}$ , and the upper and lower bound compaction rates of Mixture 3 based on the model for compaction creep in a mixture by pressure solution.

Examining Figures 25-28 shows that regardless of the differences between the mixtures, all experiments

on mixtures can be quite well described using the upper and lower bound compaction rate end members of our model. Relatively simple mixtures with a bi-modal distribution (Mixture 1 and 2), behave in a similar way as the mixture consisting of 11 grain size fractions (Mixture 3). Based on the results for the mixtures, we conclude that the geometric mean of the upper and lower bound predictions gives the best estimate of the behavior of a sample with a mixed grain size or grain size distribution. Taking the average of the upper and lower bound for such a problem is a common procedure, such as the analogous example of taking the average of the Reuss and Voight bounds (Hill average) to describe elastic behavior (Hill 1965). We must however, acknowledge that for a wider range of grain sizes, especially including larger grains, our problem will become more complicated as it will result in some grains deforming in the non-linear creep regime (coarse grains), while others deform in the linear regime (fine grains). In addition, the range of grain sizes in Mixture 3 is from 70 to 500  $\mu\text{m}$  (i.e. 0.07-0.5 mm), while some of the mixtures used in previous experiments on crushed rock salt, as well as potential real backfill material, may have a grain size ranging from 0.01 to 10 mm. Therefore, it has to be evaluated whether this model can work for such wide ranges and a firmer theoretical basis for the averaging procedure needs to be sought. Nevertheless, it can be a starting point if it is desired to not have special treatment of the crushed backfill and determine how a mixture will deform based on analysis of its grain size distribution. However, it can be expected that grain size stratification is more likely to occur in a repository than in a controlled experiment. Uncertainties in compaction behavior and porosity/perm evolution associated with such stratification can perhaps be minimized by the development of uniform backfill deposition methods.

#### 4.4 The permeability of compacted rock salt

Our permeability versus porosity data is plotted together with the porosity-permeability relations obtained by Bechthold et al. (2004) (see Figure 29). Bechthold et al. (2004) indicated two regimes, one with relatively little decrease in permeability when aggregate porosity is above 10%, and one with a sharp decrease in permeability below a porosity of 10%. Although, the general trend in our data is similar to the one found by Bechthold et al. (2004), it must be noted that the permeability found in this study at low porosity clearly is one order of magnitude higher than predicted by the relations of Bechthold et al. (2004). Although our error in porosity is relatively high at low porosity, this cannot entirely account for the observed difference (see error bars). A possible explanation is that during (some of) the permeability measurements, especially those made during the early stages of the experiment, some dissolution of the sample occurred due to slight under saturation of the brine. Hence, this would increase the apparent porosity at a given sample length. It must be noted that around 1% porosity, permeability is still several orders of magnitude higher than that of undisturbed salt (i.e.  $\kappa < 10^{-21} \text{m}^2$ ). It is expected that on timescales beyond our lab timescales (i.e. days-weeks), pore occlusion by local dissolution and precipitation processes will result in further reduction of connected porosity and hence permeability (Houben et al. 2013; Zhang et al. 2007). This will be further explored in future, longer-term experiments.

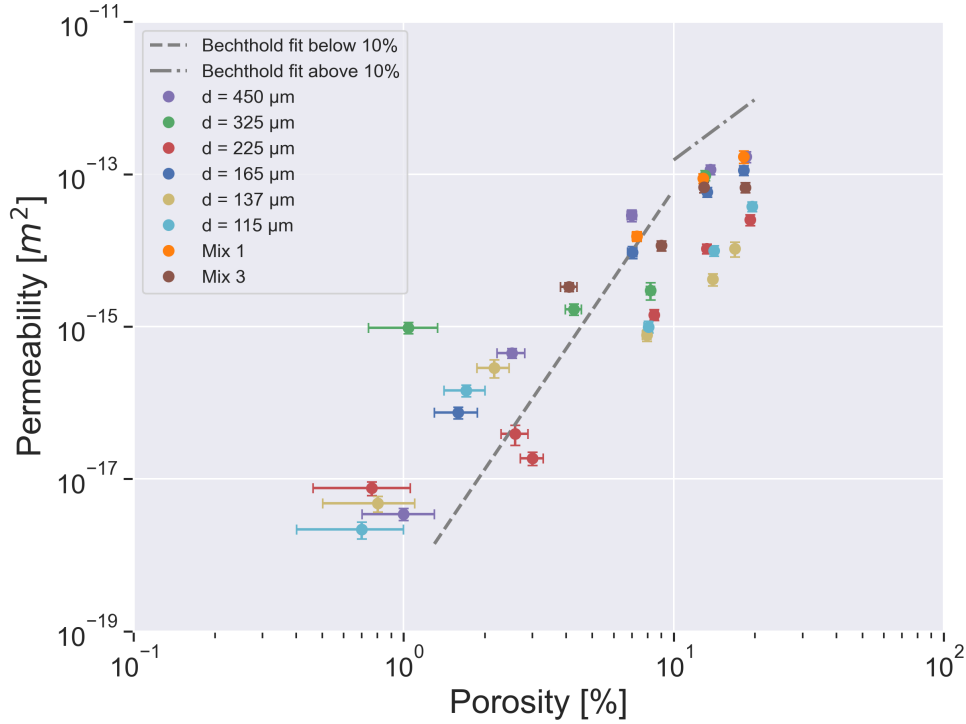


**Figure 29:** Brine permeability versus porosity for wet compacted salt. The porosity-permeability relations obtained by Bechthold et al. (2004) are shown as grey, dashed lines.

#### 4.5 A model for coupled convergence of a backfilled repository

From the previous sections, it has become clear that stress, grain size and porosity have a significant effect on the compaction rate of the backfill. In order to obtain how stress, porosity and compaction rate evolve during convergence of a repository one has to solve the problem of coupled convergence of the backfill and the surrounding host rock. For a proper solution, especially for a more complex geometry, this has to be solved using finite element modelling that incorporates constitutive laws for the salt host rock and the backfill (e.g. Kröhn et al. 2012). However, we have developed an analytical solution that can describe the convergence of a 2D cylindrical opening, surrounded by an elastic solid that also exhibits steady state creep. The framework of this solution is described in COVRA Phase 1 Deliverable (Van Oosterhout et al. 2022).

In this model we assume that steady state creep in the surrounding host rock can be described using a simple two component flow law consisting of a power law part representing dislocation creep (after Hunsche and Hampel 1999) (also see Van Oosterhout et al. (2022)) and a linear part representing pressure solution (following the approach of Spiers et al. 1990). For 2D compaction of the backfill we assume it can be described by the composite flow law derived in this study (Equation 16), which consists of the modified pressure solution creep law (Equation ?? and the empirical law established here for non-linear creep (Equation 14). Note that we have assumed that the backfill will contain only a few percent of brine, which conservatively is expected to slow down pressure solution creep by one order of magnitude compared to saturated conditions. Therefore  $A_{p>0}$  takes the value of  $6.12 \cdot 10^{-14}$  as opposed to  $6.12 \cdot 10^{-13}$  for saturated conditions. By further taking a lithostatic pressure of 15 MPa, corresponding to a repository at a depth of 700-800 m, a grain size of 5 mm in the dense surrounding rock salt, a temperature of 40°C, an initial backfill porosity of 40% and an initial 2D mean effective stress of zero, we can predict the compaction creep rate, backfill porosity and mean stress as a function of time and/or porosity. The results are presented in the next section.

##### 4.5.1 The effect of backfill grain size on repository convergence

To test the effect of grain size on compaction creep rates, we have used the analytical solution of the coupled creep model (Van Oosterhout et al. 2022) for three grain sizes: 0.3, 1.0 and 3.0 mm. A grain size of 0.3 mm is chosen because it is within the range of grain sizes on which experiments are performed in

this study and a grain size of 3.0 mm is chosen, because in our view it represent a coarse grain size that can be expected for in-situ material obtained from excavating the repository. Note that this is a very rough estimate. Grain sizes in natural dense rock salt are in the range of 2-20 mm (Urai et al. 2008) and it is likely that some grain size reduction takes place during excavation but this can vary depending on the type of equipment. The evolution of compaction rate, mean stress as a function of backfill porosity for these three grain sizes are shown in respectively Figure 30 and 31. The backfill porosity as a function of time is given in Figure 32.

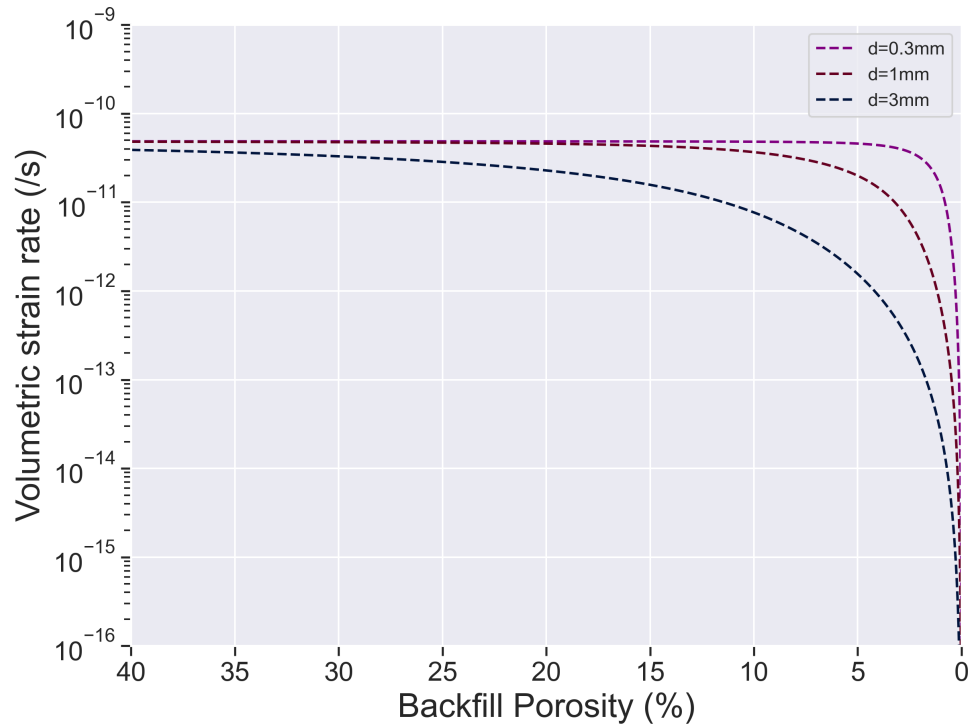


**Figure 30:** *Compaction rate versus backfill porosity for a backfill grain size of 0.3 mm, 1.0 mm and 3.0 mm, using our modified composite model (Equation 9, 14 and 16). Note that initially the strength of the backfill compared to the surrounding host rock is so low, that the convergence rate is purely determined by the convergence rate of the repository walls and in effect is equal to the convergence of an empty repository.*

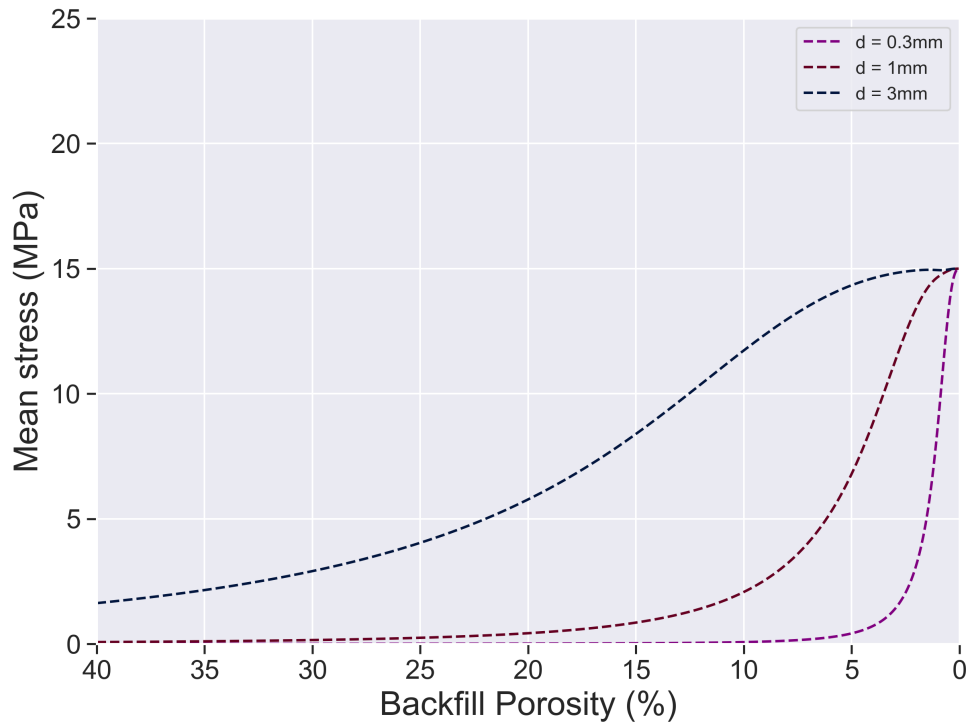


**Figure 31:** Mean stress versus backfill porosity for a backfill grain size of 0.3 mm, 1.0 mm and 3.0 mm, using our modified composite model (Equation 9, 14 and 16). Note that in the samples with a grain size of 0.3 and 1.0 mm, at a high porosity (e.g. below respectively 4 and 15%), the backfill is relatively weak compared to the host rock and the mean stress cannot increase.

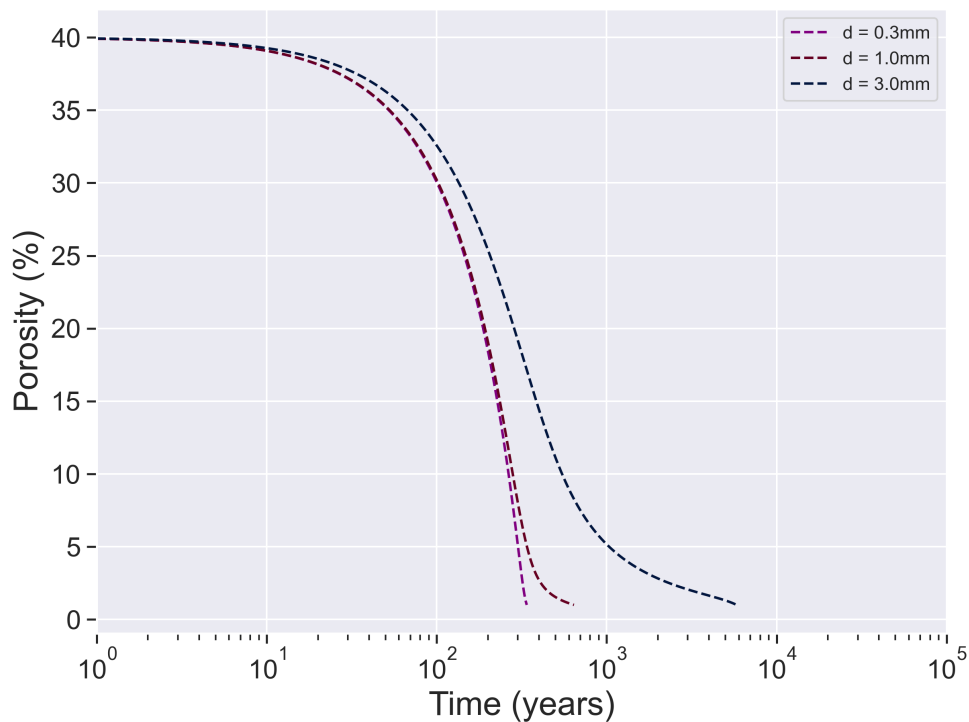


**Figure 32:** Backfill porosity versus log time, for a backfill grain size of 0.3 mm, 1.0 mm and 3.0 mm, using our modified composite model (Equation 9, 14 and 16). Note that the porosity reduction rate has been integrated until a backfill porosity of 1% is reached. Based on our model, a porosity of 1% is reached after respectively 338, 653 and 8541 years for a grain size of 0.3, 1.0 and 3.0 mm, respectively.

The results of our model show that initially (i.e. at high porosity), there is not much difference in the predicted volumetric strain rate of the backfill for different grain sizes. This can be explained by the fact that if the porosity of the backfill is very high, it is very soft compared to the surrounding dense host rock. Therefore, it is very easy to deform the backfill and the convergence is purely controlled by the rate of convergence of the surrounding host rock. Hence, initially the convergence rate can be assumed to be equal to that of an empty repository. After significant porosity reduction in the backfill, the strength of the backfill starts to increase and it can support a larger load. Hence, the mean stress will go up (see Figure 31). This will occur at an earlier stage in the backfill with a larger grain size as its resistance to compaction is higher (i.e. at a fixed imposed strain rate, the stress required for compaction is higher when the grain size is larger). Hence, intermediate to high stresses of 10-15 MPa (i.e. approaching lithostatic pressure) are only reached during the final stages of compaction when porosity is very low (<3-10%).

A key aim of using crushed backfill is that it provides a barrier as it becomes nearly impermeable when porosity is low and pore connectivity is lost. It is desirable to have a backfill that compacts in a relatively short amount of time to reduce chances of transport of radionuclides, especially when the barrier function of the waste canisters can no longer be guaranteed. Figure 32 shows that using a backfill with a small grain size substantially reduces the timescale required for the backfill to converge to a porosity of 1%, around which the permeability is expected to be around  $10^{-17} m^2$ . Timescales range from around 8000 years for a relatively coarse grain size of 3 mm, to around 300 years for a finer grain size of 0.3 mm.

Finally it is useful to evaluate which mechanisms dominate at the in-situ stresses that develop during convergence of the repository, as one has to evaluate whether the experimental results are obtained in the right stress range. In section 4.2 we have presented a deformation mechanism map for rock salt (Figure 23). Recognizing that we have modified the pressure solution creep law to account for a few percent brine present, as opposed to fully saturated conditions, we have to modify this deformation mechanism map, which we show in Figure 33.

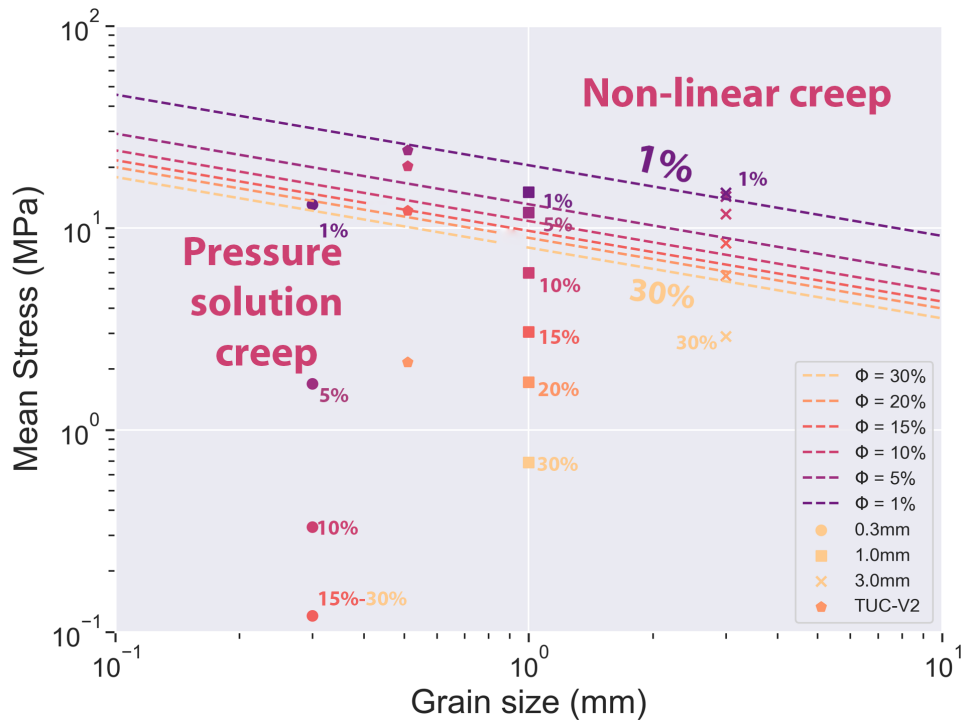


**Figure 33:** Deformation mechanism map for compaction creep in granular salt in log stress versus log grain size space for a porosity of 1-30%, for aggregates with a few % of brine (Equation 9, 14 and 16). The circles, squares and crosses indicate the mean stresses calculated at fixed levels of porosity for a grain size of 0.3, 1.0 and 3.0 mm using our coupled convergence model. The pentagons indicate the stress level of the TUC-V2 experiment on KOMPASS backfill, with an average grain size of around 0.5 mm (Friedenberg et al. 2022). Note that the KOMPASS backfill has a distributed grain size with grains ranging from 0.1 to 10 mm.

In this deformation mechanism map, we have now indicated the stress conditions for the three grain sizes of 0.3, 1.0 and 3.0 mm at a range of porosity from 30-1%. Our analysis shows that during in-situ stress conditions and porosity, non-linear creep is only expected to occur in backfill with a grain size larger than 2.0 mm. In backfill with a finer grain size, one does not have to take non-linear creep into account for estimating compaction of backfill. On the other hand if the grain size is coarse ( $> 2$  mm) it is expected that compaction of the backfill below 20% porosity will occur within the non-linear creep domain. Many of the long-term compaction experiments (e.g. Kröhn et al. 2012; Friedenberg et al. 2022) increase stress to 15-25 MPa around a porosity of 15% to obtain strain rates that are still measurable in the laboratory, such that lower aggregate porosity values can be reached within months instead of decades. As an example, the stress conditions of the TUC-V2 experiment (Friedenberg et al. 2022) are plotted in Figure 33. This experiment was performed on the KOMPASS mixture material, which has an average grain size of 0.51 mm, although having a very wide distribution of 0.01-10 mm. While for that average grain size, based on our model, it is expected that the in-situ stress conditions will entirely fall within the pressure solution creep domain. However, recognizing that this experiment has a wide grain size distribution, there is nevertheless a significant chance that the experimental results were entirely obtained in the non-linear creep domain.

A recent analysis of several coupled backfill-host rock convergence models by Friedenberg et al. (2023), showed that there is a large discrepancy in strain rates of about one order of magnitude in the range of porosity of 10-17% (see green band in Figure 34), although all of these models tested have been calibrated against the results of the TUC-V2 experiment at this same porosity range. Hence, all these models agree at the experimental conditions, but do not agree at the in-situ expected stresses. A possible explanation could be that the non-linear creep parts of these models are calibrated at these high stresses, leading to a substantial misfit when extrapolated to the in-situ stresses at which convergence occurs. Hence, the differences in the models are not apparent at high stresses (i.e. at which the experiment has been conducted) but are obvious at low stresses. In any case, it shows that care is needed when extrapolating to lower stresses.

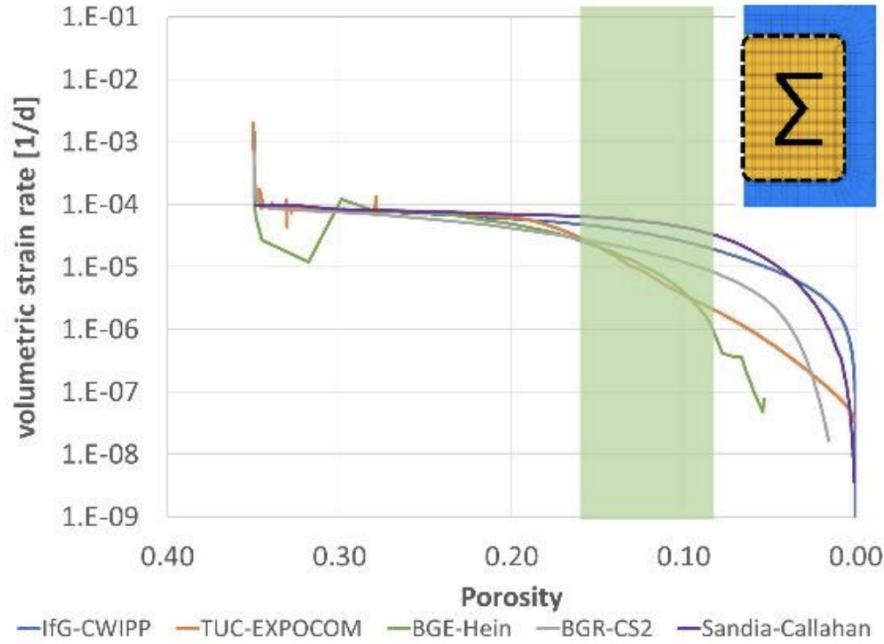


**Figure 34:** Results of the comparison of a range of constitutive equations on modelled coupled-convergence behavior after Friedenberget al. (2023). Calibrated against the TUC-V2 test. Note that the analytical solution of our coupled convergence model (Figure 30) has a similar shape as the Sandia-Callahan and IfG-CWIPP model, but is very different from the other models.

#### 4.5.2 Other effects on repository convergence

The results in the previous sections are all presented for a temperature of 40°C. This corresponds to the Dutch disposal plan to store waste for the first 100 years in an above ground facility and the heat generation of the waste does not result in significant heating of the backfill. Including heat generation will accelerate compaction creep. Furthermore, in this report we do not consider the generation of gas pressure by radiolysis and corrosion. Gas pressure build up will decrease the mean effective stress in the backfill and will reduce creep rates, assuming the gas cannot escape. The pore pressure build up, if any, is determined by the amount of gas generated, the available volume at the time of generation and the permeability/connectivity to the surroundings. Pressure build-up due to the added brine, will also lower the effective stress near the final stage of convergence.

## 5 Recommendations

The experimental results obtained in this study confirm grain size dependency observed in earlier experiments on compaction creep at low stresses (Zhang et al. 2007; Spiers et al. 1990). The experimental results show that pressure solution is the dominant mechanism at low stress and all evidence points out that it is the dominant backfill compaction mechanism when grain size is below 2 mm. In addition, it also highlights that extrapolation of experiments performed at high porosity results in overestimation of strain rates at low porosity and hence can result in overly optimistic timescales for convergence of a backfilled repository. On the other hand this study clearly demonstrates that when using a fine-grained material (e.g. 0.5 mm grain size or smaller) with a narrow distribution, the backfill is expected to reach a low permeability (e.g. around 1% porosity) at a timescale of around 400-500 years. Another advantage of using fine-grained material is that it is actually possible to obtain measurable strain rates in experiments at stresses that are in the same range as expected during in-situ convergence of a repository. This requires less extrapolation and further reduces the uncertainty of convergence times. Hence we highly recommend to consider using a fine-grained (0.3-0.5 mm) designer backfill to reduce the uncertainty in extrapolation and decrease the timescales for sealing. On the other hand, using grain sizes smaller than 0.3 mm hardly has any effect on further increasing the convergence rate, as by then it will be completely controlled by the convergence rate of the surrounding host rock, similar to having an 'empty' repository.

In addition we would also recommend to eventually use the constitutive laws obtained from this project to perform a full FEM analysis on convergence of a repository for a more realistic geometry and 3D stress state.

## 6 Future plans

With the experimental results of this study we have obtained more insight in the effect of porosity, stress, grain size and deformation mechanism on compaction creep rates of backfill. However, there are quite a few uncertainties that still require further thought and research. In this report, we have performed experiments under conditions where the pores were fully flooded with brine, accelerating creep rates in the experiments. When modelling convergence times we have taken into account that in a real case, only a few percent of brine will be added (as opposed to fully saturated conditions), which will lower the compaction rate by one order of magnitude. However, we still have to determine the exact true impact of the chemical environment (i.e. the relative humidity in the repository).

As such, we have to determine the effect of having humid air present in the pores as opposed to liquid brine in varying amounts. At present it is not known when, if, how and how much brine will be added to the backfill. If no brine will be added to (parts of) the repository it will slow down compaction creep significantly. Zhang et al. (2007) have shown that for truly dry conditions creep will be very slow (i.e. immeasurably slow at stresses expected for in-situ convergence), but there is also evidence in this study and by others that in the presence of lab-air creep is already significantly accelerated compared to dry conditions, indicating that the presence of even minor amounts of adsorbed water have a significant weakening effect (Zhang et al. 2007; Kröhn et al. 2012; Bechthold et al. 2004). In a repository the hygroscopic properties of rock salt will lead to adsorption of water to the backfill from its surrounding until it reaches an equilibrium humidity of 75%. Hence it is key to determine how the rock salt will behave under these conditions. Not adding brine will not result in having completely dry salt, but much more likely in having salt in contact with a humidity of around 75%. This is considerably higher than employed in most lab experiments.

So far we have not yet presented results of any microstructural analysis of the deformed samples. Hence to substantiate the mechanistic interpretation we will analyze samples compacted under specific conditions to compare the observations to the mechanical interpretation. Finally, we are currently setting up long-term healing experiments to investigate further static porosity-permeability reduction, caused by pore reconfiguration due to interfacial energy reduction. This is expected to decrease permeability from around  $10^{-17-19}m^2$  to permeability values comparable to natural undisturbed rock salt ( $< 10^{-21}m^2$ ). For these experiments both 3D/timelapse images of the aggregates and periodic permeability data will be obtained. If time allows additional experiments on mixtures will be performed to test the limits of the approach in the model discussed here. This is especially relevant if COVRA decides to not treat the crushed backfill and use the material as is after mining. Such experiments would also be useful in testing whether our approach for taking the average of the homogeneous stress and homogeneous strain rate model works for with a much wider distribution such as the Kompass distribution and perhaps can explain some of the variations observed in these experiments (e.g. Kröhn et al. 2012; Friedenberget al. 2023).

## 7 Conclusions

Experiments have been carried out to investigate the compaction behavior of fully brine-saturated granular salt aggregates. These stress relaxation experiments have proven to be very useful in determining the effect of stress, porosity and grain size on compaction rates. In summary, we found that:

1. The experiments show that creep is controlled by (linear) pressure solution creep at low stress and a non-linear creep mechanism at high stress. This is best described using Equation 9 and 14.
2. For an aggregate with a distributed grain size, compaction creep rates by pressure solution (i.e. at low stress) can be explained based on the results of compaction experiments on aggregates with single grain size fraction.

3. The geometric mean of the theoretical upper bound (homogeneous stress) and lower bound (homogeneous strain rate) compaction rate gives a good estimate for the compaction behavior of a mixture.
4. Although the non-linear creep mechanism is not fully understood, we have shown with our coupled convergence model that for in-situ conditions pressure solution creep is likely to be the dominant mechanism in a compacting backfill. In case the backfill contains only a few percent brine present, or has humid air in the pores, further experiments are required to assess which compaction mechanisms will dominate during compaction and under which conditions (stress, porosity, grain size).
5. Based on the experiments and constitutive laws put forward in this study it is expected that for grain sizes of 0.3 to 3.0 mm, the backfill is expected to compact to 1% porosity, reaching a low permeability, after 300 to 9000 years, respectively.

## 8 Acknowledgements

This research was funded by COVRA, the Central Organisation For Radioactive Waste. T. van der Gon, F. van Oort and G. Kuipers are thanked for technical support.

## 9 References

### References

- Bechthold, W, S Heusermann, and E Smailos. 2004. *Backfilling and Sealing of Underground Respositories for Radioactive Waste in Salt: Bambus II Project*. Publications Office of the European Union.
- Callahan, GD, KD Mellegard, and FD Hansen. 1998. *Constitutive behavior of reconsolidating crushed salt*. Technical report. Sandia National Lab.(SNL-NM), Albuquerque, NM (United States).
- Carter, NL, ST Horseman, JE Russell, and J Handin. 1993. "Rheology of rocksalt." *Journal of Structural Geology* 15 (9-10): 1257–1271.
- Czaikowski, O, K Wiczorek, and K-P Kröhn. 2012. "Compaction of salt backfill—new experiments and numerical modelling." In *Mechanical Behaviour of Salt VII*, 169–174. CRC Press.
- De Meer, Siese, Christopher J Spiers, Colin J Peach, and Tohru Watanabe. 2002. "Diffusive properties of fluid-filled grain boundaries measured electrically during active pressure solution." *Earth and Planetary Science Letters* 200 (1-2): 147–157.
- Friedenberg, Larissa, Jeroen Bartol, James Bean, Oliver Czaikowski, Uwe Dusterloh, Ann-Kathrin Gartzke, Suzanne Hangx, Ben Laurich, Christian Lerch, Svetlana Lerche, et al. 2022. "Compaction of crushed salt for safe containment: Overview of phase 2 of the KOMPASS project." *The Mechanical Behavior of Salt X*, no. 1, 283–291.
- Friedenberg, Larissa, Jeroen Bartol, James Bean, Oliver Czaikowski, Uwe Dusterloh, Ann-Kathrin Gartzke, Suzanne Hangx, Ben Laurich, Christian Lerch, Svetlana Lerche, et al. 2023. "Compaction of crushed salt for safe containment: Overview of phase 2 of the KOMPASS project."
- Gultinan, Eric J, Kristopher L Kuhlman, Jonny Rutqvist, Mengsu Hu, Hakim Boukhalfa, Melissa Mills, Shawn Otto, Douglas J Weaver, Brian Dozier, and Philip H Stauffer. 2020. "Temperature response and brine availability to heated boreholes in bedded salt." *Vadose Zone Journal* 19 (1): e20019.
- Hill, Rodney. 1965. "A self-consistent mechanics of composite materials." *Journal of the Mechanics and Physics of Solids* 13 (4): 213–222.
- Holcomb, David Joseph, and DW Hannum. 1982. *Consolidation of crushed-salt backfill under conditions appropriate to the WIPP facility*. Technical report. Sandia National Labs.
- Houben, ME, A Ten Hove, CJ Peach, and CJ Spiers. 2013. "Crack healing in rocksalt via diffusion in adsorbed aqueous films: Microphysical modelling versus experiments." *Physics and Chemistry of the Earth, parts A/B/C* 64:95–104.

- Hunsche, Udo, and Andreas Hampel. 1999. "Rock salt—the mechanical properties of the host rock material for a radioactive waste repository." *Engineering geology* 52 (3-4): 271–291.
- Koelemeijer, Paula J, Colin J Peach, and Christopher J Spiers. 2012. "Surface diffusivity of cleaved NaCl crystals as a function of humidity: Impedance spectroscopy measurements and implications for crack healing in rock salt." *Journal of Geophysical Research: Solid Earth* 117 (B1).
- Korthaus, Ekkehard. 1998. *Experiments on crushed salt consolidation with true triaxial testing device as a contribution to an EC benchmark exercise*. Vol. 6181. FZKA.
- Kröhn, K-P, CL Zhang, J Wolf, D Stührenberg, M Jobmann, L von Borstel, and C Lerch. 2012. "The compaction behaviour of salt backfill at low porosities." In *Mechanical Behaviour of Salt VII*, 175–182. CRC Press.
- Langer, M. 1999. "Principles of geomechanical safety assessment for radioactive waste disposal in salt structures." *Engineering geology* 52 (3-4): 257–269.
- Lee, Do, and EW Hart. 1971. "Stress relaxation and mechanical behavior of metals." *Metallurgical Transactions* 2:1245–1248.
- Oldenburg, Curtis M, and Karsten Pruess. 1995. "Dispersive transport dynamics in a strongly coupled groundwater-brine flow system." *Water Resources Research* 31 (2): 289–302.
- Phillips, SL. 1981. "A technical databook for geothermal energy utilization."
- Pluymakers, Anne MH, and Christopher J Spiers. 2015. "Compaction creep of simulated anhydrite fault gouge by pressure solution: theory v. experiments and implications for fault sealing." *Geological Society, London, Special Publications* 409 (1): 107–124.
- Pusch, Roland. 2009. "Geological storage of highly radioactive waste: current concepts and plans for radioactive waste disposal."
- Rutter, Ernest H, and DH Mainprice. 1978. "The effect of water on stress relaxation of faulted and unfaulted sandstone." *Rock Friction and Earthquake Prediction*, 634–654.
- Schulze, Otto. 1984. "Thermomechanical properties of irradiated rock salt." *Nuclear Instruments and Methods in Physics Research Section B: Beam Interactions with Materials and Atoms* 1 (2-3): 542–548.
- Schutjens, Peter Maarten Titus Maria. 1991. "Intergranular pressure solution in halite aggregates and quartz sands: an experimental investigation." PhD diss., Instituut voor Aardwetenschappen der Rijksuniversiteit te Utrecht.
- Spiers, CJ, and RH Brzesowsky. 1993. "Densification behaviour of wet granular salt: Theory versus experiment." 1:83–92.
- Spiers, CJ, PMTM Schutjens, RH Brzesowsky, CJ Peach, JL Liezenberg, and HJ Zwart. 1990. "Experimental determination of constitutive parameters governing creep of rock salt by pressure solution." *Geological Society, London, Special Publications* 54 (1): 215–227.
- Taylor, John. 1997. *Introduction to error analysis, the study of uncertainties in physical measurements*.
- Ter Heege, JH, JHP De Bresser, and CJ Spiers. 2004. "Composite flow laws for crystalline materials with log-normally distributed grain size: theory and application to olivine." *Journal of structural Geology* 26 (9): 1693–1705.
- Urai, JL, Zsolt Schléder, CJ Spiers, and PA Kukla. 2008. "Flow and transport properties of salt rocks." *Dynamics of complex intracontinental basins: The central European basin system*, 277–290.
- Van Oosterhout, Bart, Suzanne Hangx, Chris Spiers, and Hans De Bresser. 2022. *Preliminary recommendations for modelling compaction creep and porosity-permeability evolution in crushed salt backfill*.
- Zhang, X, C J Peach, J Grupa, and CJ Spiers. 2007. "Stress relaxation experiments on compacted granular salt: effects of water," 159–166.